Accepted Manuscript

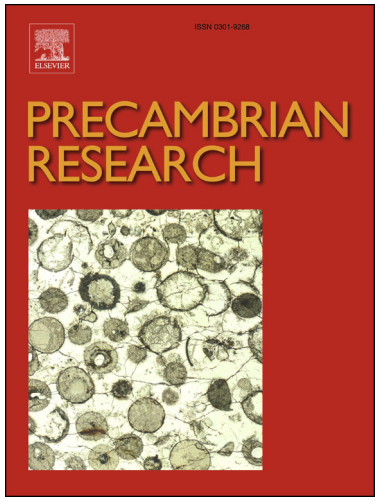

Uranium Isotope Compositions of Mid-Proterozoic Black Shales: Evidence for an Episode of Increased Ocean Oxygenation at 1.36 Ga and Evaluation of the Effect of Post-Depositional Hydrothermal Fluid Flow

Shuai Yang, Brian Kendall, Xinze Lu, Feifei Zhang, Wang Zheng

PII: S0301-9268(17)30162-6
DOI: http://dx.doi.org/10.1016/j.precamres.2017.06.016
Reference: PRECAM 4798

To appear in: *Precambrian Research*

Received Date: 25 March 2017
Revised Date: 12 June 2017
Accepted Date: 13 June 2017

Please cite this article as: S. Yang, B. Kendall, X. Lu, F. Zhang, W. Zheng, Uranium Isotope Compositions of Mid-Proterozoic Black Shales: Evidence for an Episode of Increased Ocean Oxygenation at 1.36 Ga and Evaluation of the Effect of Post-Depositional Hydrothermal Fluid Flow, *Precambrian Research* (2017), doi: http://dx.doi.org/10.1016/j.precamres.2017.06.016

Uranium Isotope Compositions of Mid-Proterozoic Black Shales: Evidence for an Episode of Increased Ocean Oxygenation at 1.36 Ga and Evaluation of the Effect of Post-Depositional Hydrothermal Fluid Flow

Shuai Yang[a], Brian Kendall[a *], Xinze Lu[a], Feifei Zhang[b], Wang Zheng[b]

[a] Department of Earth and Environmental Sciences, University of Waterloo, 200 University Avenue West, Waterloo, Ontario, Canada N2L 3G1

[b] School of Earth and Space Exploration, Arizona State University, Tempe, AZ, USA 85287

Revised manuscript submitted to *Precambrian Research*

June 12, 2017

*Corresponding author at: Department of Earth and Environmental Sciences, University of Waterloo, 200 University Avenue West, Waterloo, Ontario, Canada N2L 3G1.

Email: bkendall@uwaterloo.ca

Abstract

We report U isotope data for marine black shales of the early Mesoproterozoic Velkerri Formation (Roper Group) and late Paleoproterozoic Wollogorang Formation (Tawallah Group) from the McArthur Basin, Northern Australia. An average authigenic $\delta^{238}U$ of 0.13 ± 0.04‰ (1SD; relative to standard CRM145) was obtained for six U- and Mo-rich shales from a ~ 1 m interval that was deposited at 1361 ± 21 Ma (based on previous Re-Os geochronology). After correcting for a local U isotope fractionation of ~0.60-0.85‰ associated with U removal to anoxic sediments, we infer that global seawater at 1.36 Ga had a $\delta^{238}U$ of ~ –0.47‰ to –0.72‰, which is ~0.1-0.3‰ lighter than modern seawater (–0.39 ± 0.01‰). Uranium isotope mass-balance modelling suggests that <25% of the seafloor was anoxic at 1.36 Ga. This interpretation is consistent with high U and Mo enrichments in these samples compared with other Velkerri Formation and mid-Proterozoic black shales, which suggests a sizable dissolved oceanic Mo and U inventory developed in response to an episode of increased ocean oxygenation. Hence, a significant expanse of O_2-bearing deep ocean waters may have existed at 1.36 Ga. The O_2 concentrations of those waters were not necessarily high given that a large expanse of weakly oxygenated deep waters is also consistent with the mass-balance model. A lower average authigenic $\delta^{238}U$ of –0.08 ± 0.18‰ (1SD) was obtained for less U- and Mo-rich black shales from a ~1 m interval in the lower Velkerri Formation, deposited at 1417 ± 29 Ma. In contrast to the upper Velkerri interval, the mass-balance model permits widespread

ocean anoxia during deposition of the lower Velkerri interval.

Black shales of the ca. 1.73 Ga Paleoproterozoic Wollogorang Formation previously yielded an erroneously young Re-Os date of 1359 ± 150 Ma, likely due to post-depositional hydrothermal alteration at ca. 1640 Ma. Higher $\delta^{238}U$ is observed in samples closer to the base of the black shale unit where the greatest extent of open-system Re-Os behavior was observed. Hence, post-depositional hydrothermal fluid flow may overprint the depositional $\delta^{238}U$ of black shales and cause erroneous estimates of ancient global ocean anoxia.

Keywords: Proterozoic; ocean anoxia; uranium isotopes; Velkerri Formation; Wollogorang Formation; McArthur Basin

1. Introduction

The relationship between ocean redox conditions and the slow rates of eukaryotic evolution in the Mesoproterozoic (~1.6-1.0 Ga) oceans is an ongoing subject of debate. Iron speciation data and redox-sensitive metal (e.g., Mo, U, Cr, Zn) concentrations of mid-Proterozoic black shales indicate that the deep oceans were predominantly anoxic and Fe^{2+}-rich (ferruginous), with anoxic and H_2S-rich (euxinic) waters primarily occurring at mid-depths in regions of high primary productivity along ocean margins as well as in restricted marginal and intracratonic basins (Scott et al., 2008, 2013; Planavsky

et al., 2011; Poulton and Canfield, 2011; Boyle et al., 2013; Partin et al., 2013; Reinhard et al., 2013; Sperling et al., 2015). Chromium isotope data from ironstones and shales as well as Zn/Fe ratios in marine carbonates suggest that atmospheric O_2 levels in the Mesoproterozoic were predominantly <0.1-1.0% of present atmospheric levels (PAL) (Planavsky et al., 2014; Cole et al., 2016; Liu et al., 2016) until 1.1 Ga when larger Cr isotope fractionations suggest greater atmospheric O_2 levels (Gilleaudeau et al., 2016). Tang et al. (2016) used Ce anomaly data from carbonates and ironstones to suggest that Mesoproterozoic surface ocean O_2 concentrations were generally no more than ~0.2 μM, or about 0.1% of modern levels. Daines et al. (2017) suggested that atmospheric O_2 levels of 1-10% PAL were consistent with limited variation in the carbon isotope compositions of carbonates deposited during the Mesoproterozoic. Quantitative biogeochemical modelling by Reinhard et al. (2016) suggests pervasive deep ocean anoxia and large spatiotemporal variations in surface ocean oxygenation, particularly below ~2.5% PAL. In such a world, nitrate limitation in the open ocean may have been particularly severe, thus limiting photosynthetic eukaryotes to continental margin settings (Anbar and Knoll, 2002; Reinhard et al., 2013; Lyons et al., 2014; Koehler et al., 2017).

However, other studies suggest that a greater extent of mid-Proterozoic ocean oxygenation occurred at least episodically, such as during the early Mesoproterozoic at 1.4 Ga. Redox-sensitive metal concentrations in sedimentary rocks of the 1.4 Ga Xiamaling Formation (China) and a carbon-oxygen cycle model were used to suggest that

atmospheric O_2 levels were >4% of modern levels, implying sufficient O_2 for animal respiration long before the evolution of complex metazoans (Zhang et al., 2016). The existence of such high atmospheric O_2 levels is controversial (Planavsky et al., 2014, 2016). Nevertheless, Fe speciation, organic geochemistry, pyrite S isotope compositions, redox-sensitive metal concentrations, and eukaryotic microfossils in basinal sedimentary rocks from the Arlan Member (Kaltasy Formation, Russia) suggests that O_2-bearing deep waters were present at some places in the oceans at 1.4 Ga (Sperling et al., 2014), a conclusion also reached by Zhang et al. (2016) for the Chinese section based on redox-sensitive metal concentrations. Geochemical data from the upper Velkerri Formation (McArthur Basin, northern Australia) have also been used to suggest that an episode of increased ocean oxygenation occurred at 1.4 Ga, including elevated redox-sensitive metal enrichments in black shales (Mukherjee and Large, 2016; Cox et al., 2016).

By contrast, Cr isotope data from the upper Velkerri Formation exhibit minimal isotope fractionation relative to igneous rocks, implying atmospheric O_2 levels were sufficiently low to limit surficial Cr oxidation (Planavsky et al., 2014; Cole et al., 2016). The low atmospheric O_2 levels implied by the Cr isotope data favor widespread ocean anoxia. Not all low Cr isotope compositions, however, necessarily require low atmospheric/oceanic O_2 levels. Although most Neoproterozoic and Phanerozoic shales and ironstones have Cr isotope compositions above the igneous baseline (indicating

oxidative Cr mobilization), a small proportion also have compositions indistinguishable from this baseline, and were deposited at broadly the same time as shales and ironstones containing significantly fractionated Cr (Cole et al., 2016). The Cr isotope composition of sedimentary rocks may also be affected by the isotopic composition of riverine inputs into semi-restricted anoxic basins (the modern oceanic residence time of Cr is only ~9.5 kyr and both river and seawater Cr isotope compositions are variable; Reinhard et al., 2013; Scheiderich et al., 2015; D'Arcy et al., 2016; Gueguen et al., 2016; Paulukat et al., 2016; Wu et al., 2017), and potentially even non-redox related processes (Babechuk et al., 2017). Molybdenum isotope compositions in the upper Velkerri Formation were used to infer the global extent of ocean euxinia (Arnold et al., 2004; Kendall et al., 2009), but this proxy is not ideal for inferring the extent of general ocean anoxia (i.e., euxinic and ferruginous conditions; see Kendall and Dahl et al., 2017 for a review). Further constraints on the global extent of ocean oxygenation at 1.4 Ga using new paleoredox proxies are thus desirable.

Recently, the non-traditional U isotope system has emerged as an independent indicator for the extent of global ocean anoxia, exploiting the redox-sensitive behavior and relatively long oceanic residence time of U (~400-500 kyr) compared with the timescale of global ocean mixing (~1-2 kyr) (Stirling et al., 2007; Weyer et al., 2008; Montoya-Pino et al., 2010; Brennecka et al., 2011a, 2011b; Asael et al., 2013; Kendall et al., 2013, 2015; Andersen et al., 2014, 2015, 2016, 2017; Dahl et al., 2014; Azmy et al.,

2015; Tissot and Dauphas, 2015; Lau et al., 2016, 2017; Wang et al., 2016; Noordmann et al., 2016; Elrick et al., 2017; Lu et al., 2017). Because of the long residence time of the conservative uranyl carbonate anion ($UO_2[CO_3]_3^{4-}$) in oxygenated seawater (Ku et al., 1977; Langmuir, 1978; Dunk et al., 2002), modern open ocean seawater has a globally homogeneous $\delta^{238}U$ of –0.39 ± 0.01‰ (Stirling et al., 2007; Weyer et al., 2008; Tissot and Dauphas, 2015; Andersen et al., 2016; Noordmann et al., 2016). This seawater $\delta^{238}U$ reflects the relative extent of oxygenated versus anoxic conditions in the ocean. Reduction of U(VI) to U(IV) and its removal to modern organic-rich sediments beneath euxinic waters is associated with a large isotope fractionation (>0.4‰), which favors removal of heavier ^{238}U into sediments over lighter ^{235}U (Weyer et al., 2008; Montoya-Pino et al., 2010; Andersen et al., 2014, 2017; Noordmann et al., 2016). By comparison, U removal to sediments in other marine redox settings (strongly-oxygenated to weakly-oxygenated bottom water conditions) is associated with smaller U isotope fractionations (<0.3‰) (Weyer et al., 2008; Brennecka et al., 2011b; Romaniello et al., 2013; Goto et al., 2014; Andersen et al., 2015; Tissot and Dauphas, 2015; Chen X. et al., 2016; Noordmann et al., 2016; Wang et al., 2016). At times of more extensive ocean anoxia than today, seawater will develop lower $\delta^{238}U$ because of increased preferential burial of ^{238}U relative to ^{235}U in anoxic organic-rich sediments. Accordingly, the $\delta^{238}U$ of ancient black shales deposited during times of extensive ocean anoxia will be lower than

120 the $\delta^{238}U$ of modern organic-rich sediments (Weyer et al., 2008; Montoya-Pino et al.,
121 2010; Brennecka et al., 2011a).

122 Compared with Mo, the reduction and removal of U to anoxic sediments is less
123 dependent on dissolved H_2S availability, and is largely microbially mediated, including
124 by sulfate- and iron-reducing bacteria (Morford and Emerson, 1999; Morford et al., 2005;
125 Tribovillard et al., 2006; Algeo and Tribovillard, 2009; Stylo et al., 2015). Hence, U
126 isotopes can better constrain the global extent of general ocean anoxia than Mo isotopes.
127 In this study, we report U isotope data from black shales in the Velkerri Formation that
128 were previously analyzed for Mo and Cr isotopes (Kendall et al., 2009; Cole et al., 2016) to
129 improve constraints on the extent of global ocean anoxia at 1.4 Ga.

130 The second objective of our study is to evaluate the effect of post-depositional
131 hydrothermal fluid flow on the U isotope systematics of black shales. A geologically
132 implausible Re-Os date was obtained for black shales of the ca. 1.73 Ga Wollogorang
133 Formation, and was attributed to post-depositional hydrothermal fluid flow through these
134 shales at ca. 1640 Ma in the southern McArthur Basin (Kendall et al., 2009). Comparison
135 of the extent of open-system Re-Os behavior with Mo isotope compositions of the
136 Wollogorang Formation shales suggested that post-depositional hydrothermal fluid flow
137 can alter Mo isotope compositions from the original depositional values (Kendall et al.,
138 2009), which would cause misinterpretation of the extent of ancient ocean euxinia. In this

study, the impact of post-depositional hydrothermal fluid flow on U isotopes is evaluated using the same samples previously analyzed for Re-Os and Mo isotopes.

2. Samples

2.1 Velkerri Formation

The Velkerri Formation and the overlying McMinn Formation together represent one of a cyclic series of coarsening-upward, progradational sequences in the Roper Group that reflect deposition in a marine intracratonic basin (Roper Superbasin) influenced by tectonic activity (Fig. 1; Abbott and Sweet, 2000). The Velkerri Formation is up to 900 m thick (Ahmad et al., 2013) and consists predominantly of organic-rich black shales with subordinate organic-poor glauconitic siltstones and fine-grained sandstones (Fig. 2; Jackson and Raiswell, 1991; Warren et al., 1998; Abbott and Sweet, 2000). Organic matter in the Velkerri Formation is thermally mature (~75-150°C), indicating that the black shales are unmetamorphosed except close to a dolerite sill intrusion (Crick et al., 1988; Summons et al., 1988, 1994; Taylor et al., 1994; Warren et al., 1998; George and Ahmed, 2002).

Deposition of the black shales (total organic carbon [TOC] contents up to ~9%; Crick et al., 1988; Jackson and Raiswell, 1991; Warren et al., 1998; Mukherjee and Large, 2016) likely occurred in a quiet-water distal shelf environment (Abbott and Sweet, 2000). The formation has similar organic geochemistry as the pre-Ediacaran biomarker assemblage

facies 1 of Pawlowska et al. (2013), with high bacterial but minimal eukaryotic contributions (Flannery and George, 2014). Previous geological (e.g., sequence stratigraphy, presence of glauconite) and geochemical data (e.g., redox-sensitive metal concentrations, sequence stratigraphy, pyrite sulfur isotopes, ratios of highly reactive iron to total iron [Fe_{HR}/Fe_T], and degree of pyritization [DOP] values) from the Velkerri Formation collectively suggested that the epeiric Roper seaway was at least partially connected to the global ocean and was likely redox-stratified with low seawater sulfate concentrations (Jackson and Raiswell, 1991; Warren et al., 1998; Abbott and Sweet, 2000; Shen et al., 2003; Johnston et al., 2008; Luo et al., 2015; Mukherjee and Large, 2016; Cox et al., 2016). Water column euxinia occurred at least episodically and is thought to have been promoted by increased tectonic activity and/or increased weathering of mafic lithologies, which would have promoted increased nutrient fluxes and thus primary productivity in the Roper Superbasin (Mukherjee and Large, 2016; Cox et al., 2016).

Two Re-Os depositional ages of 1361 ± 21 Ma and 1417 ± 29 Ma were obtained for black shales from ~137-138 m (upper Velkerri Formation) and ~326-327 m depth (lower Velkerri Formation), respectively, in drill hole Urapunga-4 (Kendall et al., 2009). The Re-Os ages are stratigraphically consistent with a U-Pb zircon age of 1492 ± 4 Ma for tuff from the older Wooden Duck Member, Mainoru Formation (Jackson et al., 1999), suggesting minimal post-depositional disturbance of Re and Os (and likely also other redox-sensitive metals such as Mo and U) in the Velkerri Formation (Kendall et al.,

179 2009). These two Re-Os dated intervals are the focus of the new U isotope analyses in
180 this study.

181 Local bottom water redox conditions during the deposition of these two intervals
182 were likely different (Kendall et al., 2009). High DOP values (0.90-0.92), elevated Fe/Al
183 ratios (1.4-1.8) relative to average upper crust (~0.4-0.5; McLennan, 2001; Lyons and
184 Severmann, 2006), and pronounced enrichments in Mo (106-119 ppm) point to bottom
185 water euxinia for the ~137-138 m interval. By contrast, lower DOP values (0.43-0.51),
186 elevated Fe/Al ratios (0.5-1.4), and weaker enrichments in Mo (6-9 ppm) at ~326-327 m
187 suggest deposition from anoxic and ferruginous (Fe^{2+}-rich) waters.

188 Molybdenum isotope data from the Velkerri Formation in Urapunga-4 was used to
189 infer the global extent of ocean euxinia at ca. 1.4 Ga (Arnold et al., 2004; Kendall et al.,
190 2009). The most Mo-rich black shales (from the ~137-138 m interval) with the highest
191 DOP values (0.90-0.92), reflecting the most euxinic water column conditions, have an
192 average δ^{98}Mo of 0.95 ± 0.14‰ (2SD; re-calculated relative to standard NIST SRM 3134
193 = 0.25‰; Nägler et al., 2014) that represents a minimum value for global seawater δ^{98}Mo
194 at 1.36 Ga (any seawater-sediment Mo isotope fractionation preferentially removes lighter
195 Mo isotopes to sediments). For Mo concentrations of 106-119 ppm and seawater δ^{98}Mo of
196 ≥0.95‰, mass-balance models suggest that less than ~2% of the ca. 1.36 Ga seafloor was
197 covered by euxinic waters (Dahl et al, 2011; Reinhard et al., 2013).

198 The samples from the ~137-138 m and ~326-327 m intervals were analyzed for Cr
199 isotope compositions (Cole et al., 2016). The δ^{53}Cr values (relative to NIST SRM 979) of
200 three samples from ~137-138 m and five samples from ~326-327 m range from –0.14‰
201 to +0.05‰, and from –0.14‰ to –0.09‰, respectively, and thus are not significantly
202 different from igneous rock compositions (–0.124 ± 0.101 ‰, 2SD; Schoenberg et al.,
203 2008).
204
205 *2.2 Wollogorang Formation*
206 The ca. 1730 Ma Wollogorang Formation (Tawallah Group) was deposited in the
207 Calvert Superbasin, which was tectonically influenced by a convergent margin along the
208 southern part of the North Australian craton (Myers et al., 1996; Page et al., 2000; Scott
209 et al., 2000; Southgate et al., 2000; Betts et al., 2003). The Wollogorang Formation is
210 ~100-150 m thick and consists of dolomitic sandstone, siltstone, and mudstone, as well as
211 dolomitic organic-rich shales and dolostone (Fig. 3; Jackson, 1985; Donnelly and Jackson,
212 1988). A ~20-25 m thick unit of pyritic black shale (TOC up to ~6 wt%) containing
213 diagenetic dolomite nodules and dolomite veinlets occurs in the lower part of the
214 formation (Donnelly and Jackson, 1988; Kendall et al., 2009; Spinks et al., 2016). As for
215 the Velkerri Formation, the black shales of the Wollogorang Formation were likely
216 deposited in a low-sulfate, redox-stratified, and semi-restricted marine basin with at least
217 intermittently euxinic bottom waters based on sequence stratigraphic studies (Jackson et

al., 2000; Page et al., 2000; Southgate et al., 2000) and geochemical data (Mo enrichments, Fe_{HR}/Fe_T ratios, DOP values, and S isotopes; Shen et al., 2002; Kendall et al., 2009; Spinks et al., 2016). Multiple stratigraphic horizons of both stratiform breccia-hosted base metal sulfides and elevated whole-rock enrichments of Zn, Pb, Cu, and Tl have been found in the black shales, suggesting the Wollogorang Formation is a candidate for SEDEX (sedimentary exhalative) mineralization (Jackson, 1985; Donnelly and Jackson, 1988; Spinks et al., 2016).

Although thermal alteration of the Wollogorang Formation is restricted to sub-greenschist facies (Crick et al., 1988; Donnelly and Jackson, 1988), post-depositional hydrothermal fluid flow affected these rocks at ca. 1640 Ma (Jackson et al., 2000). Carbon isotope compositions of polycyclic aromatic hydrocarbons (PAHs) from the ca. 1640 Ma McArthur River HYC Pb-Zn-Ag ore deposit suggest an origin from the Wollogorang Formation rather than the host rocks of the Barney Creek Formation (Williford et al., 2011). In addition, an overprinted paleomagnetic pole with an age of ca. 1640 Ma was identified from the Wollogorang Formation and other Tawallah Group rocks (Idnurm et al., 1995; Idnurm, 2000). Volcanic units stratigraphically bracketing the Wollogorang Formation (the underlying Settlement Creek Volcanics and overlying Gold Creek Volcanics) have been leached of base metal sulfides and exhibit potassic alteration (Cooke et al., 1998). Hot oxidized hydrothermal fluids (T > 250°C) originating from an evaporitic environment (based on deuterium enrichment in *n*-alkanes from the HYC

238 deposit) are thought to have leached organic matter and metals out of the Wollogorang
239 Formation and other Tawallah Group rocks, ascended along the Emu Fault system, and
240 re-deposited these materials in the Barney Creek Formation (Cooke et al., 1998; Large et
241 al., 1998, 2001; Garven et al., 2001; Logan et al., 2001; Rawlings et al., 2004; Williford
242 et al., 2011).

243 Post-depositional hydrothermal fluid flow at ca. 1640 Ma disturbed the Re-Os
244 isotope systematics in the black shales of the Wollogorang Formation. A Re-Os date of
245 1359 ± 150 Ma derived from Wollogorang black shales at ~74-77 m depth in the Mount
246 Young 2 drill core (Kendall et al., 2009) is younger than U-Pb SHRIMP zircon
247 depositional ages of 1729 ± 4 Ma and 1730 ± 3 Ma for tuffaceous beds in the shales
248 (Page et al., 2000). The greatest degree of open-system Re-Os isotope behavior is found
249 in samples closest to the base of the black shale unit (suggesting fluids percolated
250 upwards from the basal contact), which have negative initial $^{187}Os/^{188}Os$ isotope ratios
251 and deviate most strongly from a ca. 1730 Ma reference isochron (Kendall et al., 2009).
252 The lowest $\delta^{98}Mo$ values (0.3‰) were also found in samples closest to the base of the
253 black shale unit, suggesting that hydrothermal fluid flow altered the $\delta^{98}Mo$ to lower
254 values relative to the original depositional signatures. Although elemental redox proxies
255 may have been affected by the hydrothermal fluid flow, the DOP values (0.57-0.92),
256 Fe/Al ratios (0.3-0.7), and Mo concentrations (41-58 ppm) in these samples imply

intermittent water column euxinia (Kendall et al., 2009; Scott and Lyons, 2012). The U isotope compositions of these samples were measured in this study.

3. Analytical Methods

A total of 20 samples from the Velkerri Formation (6 samples from 136.98-137.89 m and 5 samples from 325.71-326.69 m in Urapunga-4) and Wollogorang Formation (9 samples from 74.27-76.96 m in Mount Young 2) were analyzed for U isotope compositions. Sample dissolutions and separation of U via ion-exchange chromatography were carried out in a metal-free clean room at the Metal Isotope Geochemistry laboratory, University of Waterloo. The analytical protocols used in this study are outlined in Weyer et al. (2008) and Kendall et al. (2013), and are briefly summarized below.

A known amount (~100 mg) of sample powder was ashed overnight at 550°C in crucibles to remove organic matter, and then transferred to Savillex Teflon beakers for dissolution in concentrated HF-HNO_3-HCl at 110°C. Prior to ion-exchange chromatography, a ^{236}U-^{233}U double spike (IRMM-3636) was added to an amount of sample solution corresponding to 300 ng U to facilitate correction for instrumental mass fractionation as well as any U isotope fractionation during column chemistry. After sample-spike equilibration, U was separated from sample-spike solutions using Eichrom® UTEVA resin. The U concentrations of these samples were measured previously by Kendall et al. (2009) using quadrupole inductively coupled plasma mass

277 spectrometry. In this study, the U concentrations of the sample solutions were calculated
278 using double spike isotope dilution.

279 Uranium isotope compositions were measured on a Thermo Scientific Neptune
280 multi-collector inductively coupled plasma mass spectrometer (MC-ICP-MS) at the W.M
281 Keck Foundation Laboratory for Environmental Biogeochemistry, School of Earth and
282 Space Exploration, Arizona State University. The $\delta^{238}U$ of samples is reported as per mil
283 deviations from the CRM145 standard as follows:

284 $$\delta^{238}U\ (‰) = ({}^{238/235}U_{sample}/{}^{238/235}U_{standard} - 1) \times 1000$$

285 Over the course of this study, two secondary standards, Ricca and CRM129a, and the
286 bracketing standard CRM145 (measured against itself) yielded average $\delta^{238}U$ values of
287 –0.22 ± 0.06‰ (2SD; n=5), –1.69 ± 0.05‰ (2SD; n=5), and 0.00 ± 0.06‰ (2SD; n=56),
288 respectively. Over a 16-month period that included this study, the average $\delta^{238}U$ values for
289 Ricca and CRM129a were –0.22 ± 0.07‰ (2SD; n=243) and –1.71 ± 0.09‰ (2SD;
290 n=237), respectively. Statistically identical values for CRM129a were reported in previous
291 studies (Kendall et al., 2013, 2015). The 2SD uncertainty of a sample is either the 2SD
292 uncertainty of sample replicate measurements or 0.08‰ (the average of the long-term 2SD
293 uncertainty for Ricca and CRM129a), whichever is greater. Powder replicate analyses
294 were done for four different samples (three Velkerri samples and one Wollogorang
295 sample), and in each case yielded statistically identical $\delta^{238}U$ values given 2SD
296 uncertainties. During this study, we also measured two shale standards that were processed

297 in the same manner as samples, the United States Geological Survey (USGS) standards
298 SBC-1 and SGR-1b, and their $\delta^{238}U$ values were –0.24 ± 0.10‰ (2SD; n=3) and –0.19 ±
299 0.05‰ (2SD; n=3), respectively. Our measured $\delta^{238}U$ for SBC-1 is statistically identical to
300 the value of –0.21 ± 0.04‰ (2SD; n=3) measured by Rolison et al. (2017).
301

302 **4. Results**

303 The U and Mo concentrations, Al-normalized enrichment factors (EF =
304 $[element/Al]_{sample}$ / $[element/Al]_{average\ upper\ crust}$), and isotope compositions are reported in
305 Table 1 and illustrated in Fig. 4. Six U- and Mo-rich samples (U EF = 11-15; Mo EF =
306 168-196) from the upper Velkerri Formation have a narrow range of $\delta^{238}U$ between 0.03‰
307 and 0.12‰ (average = 0.07 ± 0.03‰; 1SD). By contrast, five U- and Mo-poor samples (U
308 EF = 2-6; Mo EF = 4-16) from the lower Velkerri Formation have lower values of $\delta^{238}U$
309 between –0.28‰ and –0.19‰ (average = –0.24 ± 0.04‰; 1SD) (Fig. 5). Nine samples
310 from the ~3 m interval in the Wollogorang Formation have variable U enrichments (EF =
311 7-24) and $\delta^{238}U$ values (–0.17‰ to +0.06‰) (Fig. 6). Distinctively different $\delta^{238}U$ are
312 observed in the upper and lower parts of the Wollogorang stratigraphic interval examined
313 in this study (Fig. 7). Five samples from 74.27-75.53 m have negative $\delta^{238}U$ values
314 between –0.17‰ and 0.00‰ (average = –0.09 ± 0.07‰; 1SD), whereas the four
315 stratigraphically lower samples from 76.00-76.96 m have positive $\delta^{238}U$ values of 0.03‰
316 to 0.06‰ (average = 0.04 ± 0.02‰; 1SD). The stratigraphic trend for the Mo isotope data

317 is opposite to that of the U isotope data, with higher δ^{98}Mo values in the 74.27-75.53 m
318 interval (Fig. 8; Kendall et al., 2009).

319 Uranium-bearing detrital minerals in a shale matrix can affect bulk sample δ^{238}U,
320 particularly if authigenic U enrichments are low. Hence, authigenic U isotope
321 compositions ($\delta^{238}U_{auth}$) were calculated using $\delta^{238}U_{auth} = \delta^{238}U_{sam} - (Al/U)_{sam} \times \{(\delta^{238}U_{det}$
322 $- \delta^{238}U_{sam})/[(Al/U)_{det} - (Al/U)_{sam}]\}$, where auth = authigenic, sam = sample, and det =
323 detrital (Asael et al., 2013). The average upper crustal values for Al (8.04 wt%) and U
324 (2.8 ppm) are used to represent the detrital U endmember (McLennan, 2001). A range of
325 detrital U isotope compositions from –0.3‰ (Tissot and Dauphas, 2015; Andersen et al.,
326 2016) to –0.8‰ (Holmden et al., 2015) are used to take into consideration that detrital U
327 could have variable δ^{238}U (e.g., preferential loss of ^{238}U during weathering; Holmden et al.,
328 2015).

329 The upper Velkerri Formation has average $\delta^{238}U_{auth}$ of 0.11 ± 0.04‰ and 0.15 ± 0.04‰
330 using $\delta^{238}U_{det}$ of –0.3‰ and –0.8‰, respectively, thus yielding an overall average of 0.13 ±
331 0.04‰ (1SD; Table 2). The calculated $\delta^{238}U_{auth}$ is only ~0.06‰ higher than bulk δ^{238}U
332 (Table 1) because the fraction of authigenic U accounts for ~91-93% of the total U. By
333 comparison, the lower Velkerri Formation has lower average $\delta^{238}U_{auth}$ of –0.21 ± 0.05‰
334 and +0.05 ± 0.17‰ using $\delta^{238}U_{det}$ of –0.3‰ and –0.8‰, respectively (overall average =
335 –0.08 ± 0.18‰; 1SD). In the lower Velkerri Formation, the detrital U accounts for 18-53%
336 of the U budget in the samples, and thus the calculated $\delta^{238}U_{auth}$ is sensitive to the assumed

337 value for $\delta^{238}U_{det}$. The five Wollogorang Formation samples from 74.27-75.53 m yield an
338 overall average $\delta^{238}U_{auth}$ of –0.04 ± 0.09‰ (1SD), whereas the four samples from
339 76.00-76.96 m have a higher overall average $\delta^{238}U_{auth}$ of 0.10 ± 0.05‰ (1SD). The fraction
340 of authigenic U is >85% for all nine Wollogorang Formation samples (with the caveat that
341 some U is potentially of post-depositional hydrothermal origin; see section 5.4).
342
343 **5. Discussion**
344 *5.1 Global seawater U isotope compositions during the early Mesoproterozoic*
345 An understanding of the local depositional environment is important for inferring
346 ancient seawater $\delta^{238}U$ using the isotopic composition of black shales, so we first review
347 the relevant factors and mechanisms prior to interpreting our data. The magnitude of U
348 isotope fractionation in anoxic settings is variable and depends on several factors,
349 including the site of U removal (water column or sediments), degree of basin restriction,
350 and microbially-mediated processes (Anderson et al., 2014, 2017). Microbial activity
351 (including iron- and sulfate-reducers) is thought to be the major mechanism for reducing
352 U(VI) to U(IV), and is associated with U isotope fractionations of 0.68‰ to 0.99‰
353 (average ~0.85‰) based on laboratory experiments (Basu et al., 2014; Stylo et al., 2015;
354 Stirling et al., 2015). A U isotope fractionation of 0.62 ± 0.17‰ was observed between
355 anoxic sediments and bottom waters in the relatively open-ocean Saanich Inlet (Holmden
356 et al., 2015). Similar U isotope fractionations of 0.6-0.8‰ were determined for the Black

Sea and Kyllaren fjord (Norway) (Noordmann et al., 2015; Rolison et al., 2017). However, the strong basin restriction in the Black Sea and Kyllaren fjord has resulted in $\delta^{238}U_{auth}$ values for the euxinic sediments that are only about ~0.4‰ higher than global seawater, reflecting slow rates of deep-water recharge and partial U drawdown in the deep waters (Weyer et al., 2008; Montoya-Pino et al., 2010; Noordmann et al., 2015). Restricted water exchange has also caused the deep waters of the Black Sea and Kyllaren fjord to have lower $\delta^{238}U$ than global seawater because of preferential ^{238}U removal to the euxinic sediments (Noordmann et al., 2015; Rolison et al., 2017).

Based on the observations from experiments and modern anoxic basins, the U isotope fractionation between seawater and relatively open-ocean (i.e., no more than moderately restricted) euxinic sediments may be 0.60-0.85‰. The lower end of this range may represent U reduction and removal from solution below the sediment-water interface such that transport-diffusion processes limit the magnitude of U isotope fractionation (Andersen et al., 2014). Uranium removal in the water column or at the sediment-water interface may be associated with a larger U isotope fractionation (Andersen et al., 2017).

The experimental data for microbially mediated U(VI) reduction (Basu et al., 2014; Stylo et al., 2015; Stirling et al., 2015) implies that U isotope fractionation may be similar in euxinic and ferruginous settings, although further studies are needed to confirm the fractionation factor for ferruginous environments. Hence, we tentatively assume a U isotope fractionation of 0.60-0.85‰ for U removal in ferruginous settings. This approach

377 is conservative because assuming a lower fractionation factor (<0.3‰) for ferruginous
378 conditions may yield an erroneously high estimate of seawater $\delta^{238}U$ and thus an
379 overestimate for the extent of global ocean oxygenation.

380 The U isotope fractionation associated with U removal to the Velkerri sediments
381 may not be affected significantly by basin restriction. The epeiric Roper seaway was
382 probably not more than moderately restricted from the global ocean based on high Mo
383 concentrations (106-119 ppm) and Mo/TOC ratios (13-16 ppm/wt%) in the euxinic upper
384 Velkerri interval. High Mo enrichments and Mo/TOC ratios in euxinic shales suggest
385 access to a large dissolved Mo reservoir (Algeo and Lyons, 2006). Notably, the Mo/TOC
386 ratios of the upper Velkerri interval are higher than those observed in euxinic sediments
387 of the more restricted Black Sea (~4.5 ppm/wt%), and intermediate between the
388 Framvaren Fjord (~9 ppm/wt%) and the less restricted Cariaco Basin (~25 ppm/wt%)
389 (Algeo and Lyons, 2006). Because seawater Mo concentrations were probably lower in
390 the mid-Proterozoic compared with today (resulting in lower overall Mo/TOC ratios in
391 euxinic shales from the mid-Proterozoic; Scott et al., 2008), the upper Velkerri Mo/TOC
392 ratios only provide a loose maximum constraint on the degree of Roper basin restriction
393 from the open ocean when comparing with Mo/TOC ratios of sediments from modern
394 semi-restricted euxinic basins. Low Mo concentrations (6-9 ppm) in the lower Velkerri
395 interval likely reflect lower rates of Mo burial during deposition from anoxic and
396 ferruginous bottom waters (as indicated by high Fe/Al ratios and low DOP values) rather

397 than a strongly restricted basin.

398 Assuming that the Roper seaway was no more than moderately restricted, then
399 applying a U isotope fractionation factor of 0.60-0.85‰ to the average $\delta^{238}U_{auth}$ of 0.13‰
400 for the upper Velkerri interval yields a global seawater $\delta^{238}U$ of –0.47‰ to –0.72‰ for ca.
401 1.36 Ga. By comparison, global seawater $\delta^{238}U$ at 1.42 Ga may have been –0.68‰ to
402 –0.93‰ based on the average $\delta^{238}U_{auth}$ of –0.08‰ for the lower Velkerri interval.

403

404 *5.2 Uranium isotope mass balance modelling of the extent of global ocean anoxia during*
405 *the early Mesoproterozoic*

406 The extent of ocean anoxia during deposition of the upper and lower Velkerri intervals
407 can be estimated through U isotope mass-balance modeling. A simple steady-state
408 mass-balance approach can be used to estimate the relative size of the anoxic U sink
409 (organic-rich sediments deposited from euxinic and ferruginous bottom waters) and all
410 other marine U sinks (pelagic/hemipelagic muds, carbonates, metalliferous sediments,
411 hydrothermally altered oceanic crust [oxic settings], and relatively more organic-rich
412 sediments deposited from weakly or mildly oxygenated bottom waters where the depth of
413 O_2 penetration below the sediment-water interface is < 1 cm [suboxic settings]; cf. Morford
414 and Emerson, 1999, Morford et al., 2005; Wang et al., 2016). The mass-balance model is
415 given by the following equation (Montoya-Pino et al., 2010):

416 $$\delta^{238}U_{input} = (f_{other} \times \delta^{238}U_{other}) + (f_{anox} \times \delta^{238}U_{anox}) \quad (I)$$

417 where input = riverine U inputs, anox = anoxic sinks, other = all other U sinks, f = the
418 fraction of U removed to each sink ($f_{other} + f_{anox} = 1$), $\delta^{238}U_{anox} = \delta^{238}U_{seawater} + \Delta_{anoxic}$, and
419 $\delta^{238}U_{other} = \delta^{238}U_{seawater} + \Delta_{other}$ (Δ = magnitude of U isotope fractionation between
420 seawater and the associated sink).

421 Rivers are the only major source of U to the modern oceans (Dunk et al., 2002). A
422 large range of $\delta^{238}U$ (–0.72‰ to +0.06‰) is observed in rivers, likely reflecting variation
423 in catchment lithology, and the overall average riverine $\delta^{238}U$ is estimated to be –0.34‰ to
424 –0.24‰ (Tissot and Dauphas, 2015; Andersen et al., 2016, 2017; Noordmann et al.,
425 2016). The riverine average is similar to the average for the upper continental crust
426 (–0.3‰), suggesting minimal net isotope fractionation during weathering at a global scale
427 (Weyer et al., 2008; Telus et al., 2012; Tissot and Dauphas, 2015; Noordmann et al., 2016)
428 despite evidence that weathered detrital material can have isotopically lighter U than the
429 upper crust (Holmden et al., 2015). Rivers at 1.4 Ga may have had broadly similar $\delta^{238}U$
430 as modern rivers because the upper continental crust likely has had a broadly similar
431 chemical composition since the end of the Archean (Andersen et al., 2015; Dhuime et al.,
432 2015; Tang et al., 2016).

433 For U sinks in the modern marine environment, the U isotope fractionation for
434 relatively open-ocean anoxic settings is assumed to be 0.60-0.85‰, as discussed
435 previously in section 5.1. A weighted average $\delta^{238}U$ (–0.36‰) and U isotope fractionation
436 (+0.04‰) from seawater can be calculated for the other (non-anoxic) sinks based on each

437 sink's U flux and isotopic composition (Table 3; Tissot and Dauphas, 2015; Andersen et al.,
438 2016; Wang et al., 2016). Similar magnitudes of isotope fractionation for the anoxic and
439 non-anoxic sinks has been assumed for ancient oceans (Montoya Pino et al., 2010;
440 Brennecka et al., 2011). If the extent of ocean anoxia was greater at 1.4 Ga than today, then
441 the extent of suboxic ocean floor was potentially also greater, whereas the extent of
442 oxygenated ocean floor was smaller. In this scenario, the overall U isotope fractionation
443 factor for the other sink may be slightly higher (e.g., 0.1‰, similar to the suboxic
444 fractionation factor; Weyer et al., 2008; Andersen et al., 2016).

445 The $\delta^{238}U_{anox}$ at 1.36 Ga is based on the average $\delta^{238}U_{auth}$ of the upper Velkerri shales
446 (0.13‰). For seawater $\delta^{238}U$ of –0.47‰ to –0.72‰, $\delta^{238}U_{other}$ is calculated to be –0.43‰
447 to –0.68‰, respectively, assuming a fractionation factor of +0.04‰ (Table 3). Solving the
448 mass-balance equation for f_{anox} yields 23-47%, and thus f_{other} is 53-77%. Alternatively,
449 assuming a fractionation factor of 0.10‰ for the other sink yields $\delta^{238}U_{other}$ of –0.37‰ to
450 –0.62‰, and thus f_{anox} and f_{other} would comprise 14-43% and 57-86% of U removal from
451 the oceans at 1.36 Ga, respectively. These simple calculations suggest that the anoxic U
452 sink at 1.36 Ga was roughly 2-7 times larger compared with the modern ocean (7-10%).

453 A greater proportion of riverine U may have been removed into anoxic sediments
454 during deposition of the lower Velkerri interval at 1.42 Ga. For seawater $\delta^{238}U$ of –0.68‰
455 to –0.93‰, $\delta^{238}U_{other}$ is –0.64‰ to –0.89‰, respectively, for a fractionation factor of
456 +0.04‰. When $\delta^{238}U_{anox}$ = –0.08, then f_{anox} and f_{other} are calculated to be 61-73% and

27-39%, respectively. If a fractionation factor of 0.10‰ is used for the other sinks, then $\delta^{238}U_{other}$ is –0.58‰ to –0.83‰, and f_{anox} and f_{other} are 56-71% and 29-44%, respectively. Hence, the anoxic U sink at 1.42 Ga may have been 6-10 times larger compared with the modern ocean. The range of possible f_{anox} and f_{other} does not account for the uncertainty on the average $\delta^{238}U_{auth}$. Consequently, the estimated magnitude of each U sink is associated with a large uncertainty for the lower Velkerri interval, which has a significantly larger 1SD (0.18‰) for average $\delta^{238}U_{auth}$ compared with the upper Velkerri interval (0.04‰).

Although commonly used, the above model is an oversimplification of the oceanic U isotope mass balance (for example, U burial fluxes are not scaled to the size of the seawater U reservoir) and does not provide meaningful information on the area of seafloor covered by different redox regimes. To infer the areal extent of seafloor anoxia during deposition of the upper and lower Velkerri intervals, we used the recent U isotope model of Wang et al. (2016). The model is summarized below, with full details provided in Wang et al. (2016).

The global seawater U concentration can be expressed as the difference between riverine input flux and total U output flux to the seafloor (Goto et al., 2014):

$$dM_{SW}/dt = F_r - \Sigma F_i \quad \text{(II)}$$

where M_{SW} is the seawater U mass, F_r is the riverine input flux (mol/yr), and ΣF_i is the total U output flux to anoxic, suboxic, and oxic sinks (mol/yr). Similarly, the seawater

$\delta^{238}U$ can be expressed as:

$$d(M_{SW}\,\delta_{SW}) / dt = F_r\,\delta_r - \Sigma F_i\,(\delta_{SW} + \Delta_i) \quad \text{(III)}$$

where δ_{SW} and δ_r are the seawater $\delta^{238}U$ and river $\delta^{238}U$, respectively, and Δ_i is the U isotope fractionation between seawater and each sink (anoxic, suboxic, and oxic; see Table 4). Assuming steady-state conditions, then dM_{SW}/dt and $d(M_{SW}\,\delta_{SW})/dt$ are both zero (Andersen et al., 2016) and equations (II) and (III) become:

$$F_r = \Sigma F_i \quad \text{(IV)}$$

$$\delta_{SW} = \delta_r - \Sigma f_i\,\Delta_i \quad \text{(V)}$$

where f_i is the fraction of the U burial flux in each sink with respect to the river input (F_i / F_r). If a first-order relationship exists between each sink's burial flux and the global seawater U concentration (Partin et al., 2013; Reinhard et al., 2013), then:

$$F_i = k_i\,A_i\,[U] \quad \text{(VI)}$$

where A_i is the areal extent of seafloor for each U sink; [U] is the seawater U concentration, and k_i is an effective burial rate constant for each sink based on its modern seafloor area and burial flux (see Table 4 for values used in the model). It then follows that:

$$\delta_{SW} = \delta_r - \frac{[A_{anoxic}*k_{anoxic}*\Delta_{anoxic} + A_{suboxic}*k_{suboxic}*\Delta_{suboxic} + A_{oxic}*k_{oxic}*\Delta_{oxic}]}{[A_{anoxic}*k_{anoxic} + A_{suboxic}*k_{suboxic} + A_{oxic}*k_{oxic}]} \quad \text{(VII)}$$

The areal extent of anoxic seafloor was calculated for a range of possible suboxic seafloor areas (from the modern area of 6% up to a maximum of 100%) that may have

497 occurred in the global ocean at 1.4 Ga (Fig. 9). For both the upper and lower Velkerri
498 intervals, the anoxic seafloor area was calculated assuming two end-member local and
499 global anoxic fractionation factors (0.60‰ and 0.85‰), based on observations in modern
500 anoxic environments and experiments with microbially-mediated reduction of U(VI) to
501 U(IV) (Weyer et al., 2008; Montoya-Pino et al., 2010; Andersen et al., 2014; Basu et al.,
502 2014; Holmden et al., 2015; Noordmann et al., 2015; Stylo et al., 2015; Stirling et al.,
503 2015; Rolison et al., 2017). General trends from this model include: 1) seawater $\delta^{238}U$
504 decreases as the anoxic seafloor area increases; 2) seawater $\delta^{238}U$ decreases as the
505 suboxic seafloor area decreases at a constant areal extent of anoxic seafloor; 3) for a
506 constant seawater $\delta^{238}U$, a greater anoxic seafloor area is calculated for higher areas of
507 suboxic seafloor (thus the oxic seafloor area must decrease); 4) using a higher U isotope
508 fractionation factor for local removal of U to anoxic sediments yields a lower global
509 seawater $\delta^{238}U$ and thus a greater areal extent of ocean anoxia; and 5) using a higher U
510 isotope fractionation factor for the global anoxic sink results in a lower estimate for the
511 areal extent of ocean anoxia.

512 For the upper Velkerri interval, assuming a global anoxic fractionation factor of 0.60‰
513 yields an anoxic seafloor area of <3% if seawater $\delta^{238}U$ was –0.47‰, and <25% when
514 seawater $\delta^{238}U$ was –0.72‰ (Fig. 9). If we assume a global anoxic fractionation factor of
515 0.85‰, then an anoxic seafloor area of <3% and <20% is calculated for seawater $\delta^{238}U$ of
516 –0.47‰ and –0.72‰, respectively. Considering the maximum areal extent of euxinic

517 seafloor (~2%) suggested by Mo mass balance models (see section 2.1), the higher
518 estimates of seafloor anoxia derived from the U mass balance model implies that most of
519 the anoxic seafloor was ferruginous. The maximum extent of anoxic seafloor area (nearly
520 25%) implied by the model is ~70 times larger than the modern anoxic seafloor area
521 (0.35%), which nevertheless comprises a relatively small fraction of the seafloor. Hence,
522 much of the seafloor was covered by oxic and suboxic waters during deposition of the
523 upper Velkerri interval. It is noted that if the local anoxic fractionation factor was <0.6‰
524 because the extent of restriction between the Roper seaway and open ocean was
525 underestimated, then a greater extent of ocean oxygenation would be inferred from the
526 mass balance model.

527 By comparison, the lower average $\delta^{238}U_{auth}$ (–0.08 ± 0.18‰) of the lower Velkerri
528 interval is consistent with a greater areal extent of ocean anoxia. If the global anoxic
529 fractionation factor was 0.60‰, then an anoxic seafloor area of <20% and up to 100% is
530 calculated for seawater $\delta^{238}U$ of –0.68‰ and –0.93‰, respectively. If the global anoxic
531 fractionation factor was 0.85‰, then an anoxic seafloor area of <20% and <40% is
532 calculated for seawater $\delta^{238}U$ of –0.68‰ and –0.93‰, respectively. Hence, the U isotope
533 mass balance model permits the possibility of widespread coverage of the global seafloor
534 by anoxic waters (of predominantly ferruginous character; Planavsky et al., 2011;
535 Reinhard et al., 2013) during deposition of the lower Velkerri interval at 1.42 Ga. By

536 contrast, the U model does not suggest widespread coverage of the global seafloor by
537 anoxic waters during deposition of the upper Velkerri interval at 1.36 Ga.
538
539 *5.3 Transient episode of ocean oxygenation at 1.36 Ga*
540 Our estimate for seawater $\delta^{238}U$ during the upper Velkerri interval (–0.47‰ to
541 –0.72‰) does not reach values as low as some estimates for seawater $\delta^{238}U$ during
542 Phanerozoic intervals characterized by more extensive ocean anoxia than today (about
543 –0.60‰ to –0.90‰), including the late Katian in the Ordovician (Lu et al., 2017), the
544 Cretaceous Oceanic Anoxic Event 2 (Montoya-Pino et al., 2010), and the late Permian
545 (Brennecka et al., 2011a; Lau et al., 2016; Elrick et al., 2017). Hence, the upper Velkerri
546 interval was potentially deposited at a time of greater ocean oxygenation compared to
547 some anoxic Phanerozoic intervals.
548 The upper Velkerri Formation may have been deposited at a time of greater ocean
549 oxygenation compared with the lower Velkerri Formation. Uranium isotope data covering
550 the entire stratigraphy of the Velkerri Formation in the Urapunga-4 core could not be
551 presented because samples were originally collected only with Re-Os geochronology in
552 mind (Kendall et al., 2009). Despite this shortcoming, the 1 m interval in the upper
553 Velkerri interval analyzed in this study is of key strategic importance in that it captures
554 higher Mo and U concentrations compared with other euxinic shales in Urapunga-4 and
555 most other mid-Proterozoic euxinic black shales (Fig. 4; Scott et al., 2008; Partin et al.,

556 2013; Mukherjee and Large, 2016). Similarly, an interval of high Mo and U
557 concentrations was also observed in euxinic shales from the thicker Velkerri Formation in
558 the Altree 2 drill core (Cox et al., 2016), which are potentially correlative with the
559 interval of peak Mo and U enrichment in Urapunga-4. These higher U and Mo
560 enrichments point to a larger dissolved oceanic inventory of Mo and U, which in turn
561 implies a smaller extent of anoxic seafloor where these metals are most efficiently
562 removed to sediments (i.e., slower Mo and U burial rates occur in weakly- to
563 strongly-oxygenated settings; Scott et al., 2008; Partin et al., 2013). Hence, the elemental
564 record and U isotope data together suggest that the upper Velkerri Formation captures a
565 transient episode of ocean oxygenation at ca. 1.36 Ga. Geochemical data from
566 sedimentary rocks of broadly similar age in Russia and China are consistent with this
567 hypothesis (Sperling et al., 2014; Zhang et al., 2016). Given uncertainties in depositional
568 age constraints, it is not clear if there were one or more short-lived oxygenation episodes
569 around 1.4 Ga.

570 It is important to note that despite the relatively small extent of seafloor anoxia
571 during the upper Velkerri oxygenation event, the U isotope mass balance model does not
572 require high O_2 levels in the O_2-bearing deep waters. The model permits the possibility
573 that non-anoxic portions of the seafloor were covered predominantly by weakly
574 oxygenated waters. This scenario is potentially compatible with the low $\delta^{53}Cr$ signatures
575 (–0.14‰ to +0.05‰; Cole et al., 2016) in the upper Velkerri Formation, which are

576 similar to igneous rock compositions (average $\delta^{53}Cr$ = –0.124 ± 0.101 ‰, 2SD;
577 Schoenberg et al., 2008), and thus suggest low atmospheric O_2 levels (<0.1-1.0% of
578 modern levels) and limited Cr-Mn redox cycling (Planavsky et al., 2014, 2016; Cole et al.,
579 2016). Sedimentary rocks with higher $\delta^{53}Cr$ than the igneous baseline are thought to
580 reflect pronounced Cr-Mn redox cycling and higher atmospheric O_2 levels (Crowe et al.,
581 2013; Planavsky et al., 2014; Cole et al., 2016).

582 It is possible, however, that environmental O_2 levels were somewhat higher than
583 implied by the low $\delta^{53}Cr$ for the upper Velkerri interval. A small, but non-trivial,
584 proportion of Neoproterozoic and Phanerozoic shales and ironstones have low $\delta^{53}Cr$ at or
585 near the igneous baseline, and were deposited broadly coeval with rocks containing
586 higher $\delta^{53}Cr$. Recent studies demonstrate that modern seawater has variable $\delta^{53}Cr$ and,
587 importantly, that seawater in semi-restricted basins can have lower $\delta^{53}Cr$ compared with
588 open-ocean seawater (the modern oceanic residence time of Cr is only ~9.5 kyr; Reinhard
589 et al., 2013; Scheiderich et al., 2015; Gueguen et al., 2016; Paulukat et al., 2016). Notably,
590 seawater in the Baltic Sea reaches $\delta^{53}Cr$ values as low as 0.13‰, significantly lower than
591 seawater in the adjoining open North Sea (0.94-1.02‰; Paulukat et al., 2016). Some
592 modern rivers have $\delta^{53}Cr$ only slightly higher than their bedrock sources, suggesting
593 single-stage oxidation of Cr(III) to Cr(VI) dominates during weathering (with an
594 associated Cr isotope fractionation of ~0.1-0.3‰) without significant back-reduction to
595 Cr(III) (D'Arcy et al., 2016; Wu et al., 2017). Hence, it is possible that sedimentary rocks

596 deposited in a relatively well-oxygenated world might contain $\delta^{53}Cr$ that is only weakly
597 fractionated relative to igneous rocks, even if such instances are relatively rare.

598 These observations, together with the greater sensitivity of Cr isotopes to partial
599 basin restriction than U isotopes (the modern oceanic residence time of U is between 1
600 and 2 orders of magnitude longer than Cr), suggest that local depositional factors may
601 explain the low $\delta^{53}Cr$ in the upper Velkerri euxinic sediments. Just as seawater $\delta^{53}Cr$ was
602 closely captured by euxinic sediments in the Cariaco Basin (Reinhard et al., 2014;
603 Gueguen et al., 2016), the $\delta^{53}Cr$ of the upper Velkerri euxinic shales may capture Roper
604 seawater $\delta^{53}Cr$. The low $\delta^{53}Cr$ of the upper Velkerri euxinic shales may reflect the input
605 of freshwater with low $\delta^{53}Cr$. If the regional bedrock sources to rivers draining into the
606 Roper seaway had $\delta^{53}Cr$ at the low half of the observed range for igneous rocks, and
607 single-stage oxidation of Cr(III) to Cr(VI) dominated during weathering, then the Roper
608 seawater and upper Velkerri euxinic shales may have had $\delta^{53}Cr$ that was not appreciably
609 different from the igneous baseline. In that scenario, atmospheric O_2 levels during the
610 upper Velkerri oxygenation event could have been higher (>0.1-1.0% of modern levels)
611 than previously suggested. In summary, the low $\delta^{53}Cr$ signatures of the upper Velkerri
612 euxinic shales are not incompatible with the U isotope evidence for a transient
613 oxygenation event at 1.36 Ga.

614

615 *5.4 Disturbance of U isotopes in the Wollogorang Formation by post-depositional*

hydrothermal fluid flow

To evaluate the effect of post-depositional hydrothermal fluid flow on the U isotope compositions of the Wollogorang Formation, we compared the Re-Os and U isotope data. A Re-Os isochron date of 1359 ± 150 Ma was derived from linear regression of all Wollogorang Formation samples (Kendall et al., 2009), and is erroneously young when compared with the U-Pb zircon depositional ages of 1729 ± 4 Ma and 1730 ± 3 Ma for tuffaceous beds in the formation (Page et al., 2000). The initial $^{187}Os/^{188}Os$ from the regression (3.5 ± 1.5) is higher than reasonable $^{187}Os/^{188}Os$ values for upper continental crust during the Paleoproterozoic (which should have had lower $^{187}Os/^{188}Os$ than the modern upper crustal average of 0.8-1.4; Esser and Turekian, 1993; Peucker-Ehrenbrink and Jahn, 2001; Hattori et al., 2003; Chen K. et al., 2016). This observation is implausible because there is no large solid Earth reservoir more radiogenic than the upper continental crust (Kendall et al., 2009).

The Re-Os isotope compositions of black shales from 76.00-76.96 m in the Mount Young 2 drill core (closest to the base of the Wollogorang black shale unit) were affected more by post-depositional hydrothermal fluid flow than the black shales from 74.18-75.53 m. Larger deviations from a ca. 1730 Ma reference Re-Os isochron were observed for samples from 76.00-76.96 m relative to 74.18-75.53 m (Kendall et al., 2009). This observation is reflected by contrasting Re-Os dates of 1781 ± 190 Ma and 1234 ± 370 Ma for 74.18-75.53 m and 76.00-76.96 m, respectively. The Re-Os date from 74.18-75.53

636 m is consistent with the U-Pb zircon ages and thus is geologically reasonable, but the
637 Re-Os date from 76.00-76.96 m is erroneously young (Page et al., 2000; Kendall et al.,
638 2009).

639 Black shales from 76.00-76.96 m have higher $\delta^{238}U_{auth}$ (0.10 ± 0.05‰) than black
640 shales from 74.27-75.53 m (–0.04 ± 0.09‰). An unpaired *t* test confirms that the difference
641 in $\delta^{238}U$ between the two intervals is statistically significant (two-tailed *p* value of 0.0279).
642 Using the Re-Os isotope data as a guide to the extent of open-system behavior, we suggest
643 that post-depositional hydrothermal fluid flow altered the $\delta^{238}U$ of at least the black shales
644 at 76.00-76.96 m to higher values relative to the original depositional values.

645 By contrast, there is no correlation between $\delta^{238}U$ and U abundances (Fig. 7) and an
646 unpaired *t* test shows that the U EFs for samples from 74.27-75.53 m and 76.00-76.96 m
647 are not significantly different (two-tailed *p* value of 0.8149). However, variability in
648 authigenic U enrichments in the Wollogorang Formation may have masked the effect of
649 post-depositional hydrothermal fluid flow on the U concentrations of the black shales.

650 Oxidizing hydrothermal fluids are suggested to have leached metals and organic
651 matter out of the Wollogorang Formation and deposited these materials in the Barney
652 Creek Formation during formation of the McArthur River HYC Pb-Zn-Ag deposit at ca.
653 1640 Ma (Cooke et al., 1998; Large et al., 1998, 2001; Garven et al., 2001; Logan et al.,
654 2001; Rawlings et al., 2004; Williford et al., 2011). The samples exhibiting the greatest
655 extent of open-system behavior with respect to Re-Os isotopes have the highest $\delta^{238}U$

656 (this study) and lowest δ^{98}Mo (Kendall et al., 2009) (Fig. 8). Hence, oxidizing
657 hydrothermal fluids may have preferentially leached lighter U isotopes and heavier Mo
658 isotopes out of the Wollogorang Formation. Alternatively, the black shales were reducing
659 traps for Mo and U carried by the hydrothermal fluids. Based on the observed isotopic
660 trends in the Wollogorang black shale unit, this alternative scenario caused preferential
661 addition of isotopically heavier U and isotopically lighter Mo to the Wollogorang shales,
662 consistent with the observed direction of isotope fractionation during Mo and U removal
663 from the water column to organic-rich sediments in modern anoxic basins (e.g., Neubert et
664 al., 2008; Weyer et al., 2008).

665 Our data suggest that post-depositional hydrothermal fluid flow can shift the δ^{238}U
666 and δ^{98}Mo of black shales to higher and lower values, respectively, compared with original
667 depositional signatures. Consequently, the Wollogorang shales may yield an erroneous
668 underestimate and overestimate of the global extent of ocean anoxia and euxinia using U
669 and Mo isotope data, respectively. It is noted that we cannot exclude the possibility that
670 the different δ^{238}U of the 74.27-75.53 m and 76.00-76.96 m intervals reflects a change in
671 ocean redox conditions rather than hydrothermal alteration. However, it is not advisable
672 to assume U (and Mo) isotope data from black shales represent depositional signatures
673 when there is clear evidence of open-system behavior for Re-Os isotopes from the same
674 shales due to post-depositional hydrothermal fluid flow.

675

6. Conclusions

An average $\delta^{238}U_{auth}$ of 0.13 ± 0.04‰ from a ~1 m interval in the upper Velkerri Formation (drill hole Urapunga-4) suggests that seawater $\delta^{238}U$ at 1.36 Ga was ~ –0.47‰ to –0.72‰, assuming an isotope fractionation of 0.60-0.85‰ during local U removal to sediments. A lower seawater $\delta^{238}U$ of ~ –0.68‰ to –0.93‰ at 1.42 Ga may have occurred during deposition of a 1 m interval in the lower Velkerri Formation, based on its average $\delta^{238}U_{auth}$ of –0.08 ± 0.18‰. Uranium isotope mass-balance modeling suggests that <25% of the seafloor was anoxic during deposition of the upper Velkerri interval, whereas more widespread seafloor anoxia may have existed during deposition of the lower Velkerri interval. Hence, a transient episode of increased ocean oxygenation may have occurred at 1.36 Ga. This oxygenation event can explain higher Mo and U concentrations (suggestive of a higher dissolved Mo and U inventory in the oceans) in the upper Velkerri interval than other euxinic shales in the Velkerri Formation as well as other mid-Proterozoic euxinic shales. Sedimentary rocks from Russia and China that yield geochemical evidence for O_2-bearing deep waters potentially capture the same oxygenation event recorded in the upper Velkerri Formation, but the uncertainties in depositional age constraints for these three different localities means that multiple oxygenation events around 1.4 Ga are also possible.

Comparison of the extent of open-system Re-Os isotope systematics with U isotope data for black shales of the Wollogorang Formation suggests that hydrothermal alteration

696 affected U isotope compositions. Higher $\delta^{238}U$ near the base of the Wollogorang black
697 shale unit suggests that isotopically heavy U was added to the shales via U reductive
698 capture or that isotopically lighter U was leached from the shales by hydrothermal fluids.
699 Hence, hydrothermal alteration of black shale U isotope compositions, if not recognized,
700 will lead to erroneous interpretations of ocean paleoredox conditions.
701

702 **Acknowledgements**

703 This study was funded by a NSERC Discovery Grant (RGPIN-435930) to Kendall.
704 Liyan Xing is thanked for assistance with chemical processing of the samples prior to
705 mass spectrometry. The samples analyzed in this study were originally collected with
706 Robert Creaser for Re-Os geochronology. Randall Parrish is thanked for editorial
707 handling.
708

709 **References**

710 Abbott, S.T., Sweet I.P., 2000. Tectonic control on third-order sequences in a siliciclastic
711 ramp-style basin: an example from the Roper Superbasin (Mesoproterozoic),
712 northern Australia. Australian Journal of Earth Sciences 47, 637-657.
713 Ahmad, M., Dunster, J.N., Munson, T.J., 2013. Chapter 15: McArthur Basin, in: Ahmad,
714 M., Munson, T.J., (compilers), Geology and Mineral Resources of the Northern
715 Territory. Northern Territory Geological Survey. Special Publication 5.

716 Algeo, T.J., Lyons, T.W. 2006. Mo–total organic carbon covariation in modern anoxic
717 marine environments: Implications for analysis of paleoredox and
718 paleohydrographic conditions. Paleoceanography 21. PA1016.
719 Algeo, T.J., Tribovillard, N., 2009. Environmental analysis of paleoceanographic systems
720 based on molybdenum-uranium covariation. Chemical Geology 268, 211-225.
721 Anbar, A.D., Knoll, A.H., 2002. Proterozoic ocean chemistry and evolution: A
722 bioinorganic bridge? Science 297, 1137-1142.
723 Andersen, M.B., Elliott, T., Freymuth, H., Sims, K.W., Niu, Y., Kelley, K.A., 2015. The
724 terrestrial uranium isotope cycle. Nature 517, 356-359.
725 Andersen, M.B., Romaniello, S., Vance, D., Little, S.H., Herdman, R., Lyons, T.W.,
726 2014. A modern framework for the interpretation of $^{238}U/^{235}U$ in studies of ancient
727 ocean redox. Earth and Planetary Science Letters 400, 184-194.
728 Andersen, M.B., Vance, D., Morford, J.L., Bura-Nakić, E., Breitenbach, S.F.M., Och, L.,
729 2016. Closing in on the marine $^{238}U/^{235}U$ budget. Chemical Geology 420, 11-22.
730 Andersen, M.B., Stirling, C.H., Weyer S., 2017. Uranium isotope fractionation. Reviews
731 in Mineralogy and Geochemistry 82, 799-850.
732 Arnold, G.L., Anbar, A.D., Barling, J., Lyons, T.W., 2004. Molybdenum isotope
733 evidence for widespread anoxia in Mid- Proterozoic oceans. Science 304, 87-90.
734 Asael, D., Tissot, F.L.H., Reinhard, C.T., Rouxel, O., Dauphas, N., Lyons, T.W.,
735 Ponzevera, E., Liorzou, C., Chéron, S., 2013. Coupled molybdenum, iron and

736 uranium stable isotopes as oceanic paleoredox proxies during the Paleoproterozoic
737 Shunga Event. Chemical Geology 362, 193-210.
738 Azmy, K., Kendall, B., Brand, U., Stouge, S., Gordon, G.W., 2015. Redox conditions
739 across the Cambrian-Ordovician boundary: Elemental and isotopic signatures
740 retained in the GSSP carbonates. Palaeogeography Palaeoclimatology
741 Palaeoecology 440, 440-454.
742 Babechuk, M.G., Kleinhanns, I.C., Schoenberg, R., 2017. Chromium geochemistry of the
743 ca. 1.85 Ga Flin Flon paleosol. Geobiology 15, 30-50.
744 Barnes, C.E., Cochran J.K., 1990. Uranium removal in oceanic sediments and the oceanic
745 U balance. Earth and Planetary Science Letters 97, 94-101.
746 Basu, A., Sanford, R.A., Johnson, T.M., Lundstrom, C.C., Löfler, F.E., 2014. Uranium
747 isotopic fractionation factors during U(VI) reduction by bacterial isolates.
748 Geochimica et Cosmochimica Acta 136, 100-113.
749 Betts, P.G., Giles, D., Lister, G.S., 2003. Tectonic environment of shale-hosted massive
750 sulfide Pb–Zn–Ag deposits of Proterozoic northeastern Australia. Economic
751 Geology 98, 557-576.
752 Boyle, R.A., Clark, J.R., Poulton, S.W., Shields-Zhou, G., Canfield, D.E., Lenton, T.M.,
753 2013. Nitrogen cycle feedbacks as a control on euxinia in the mid-Proterozoic ocean.
754 Nature Communications 4:1533; DOI: 10.1038/ncomms2511, 1-10.

755 Brennecka, G.A., Herrmann, A.D., Algeo, T.J., Anbar, A.D., 2011a. Rapid expansion of
756 ocean anoxia immediately before the end-Permian mass extinction. Proceedings of
757 the National Academy of Sciences U.S.A. 108, 17631-17634.
758 Brennecka, G.A., Wasylenki, L.E., Bargar, J.R., Weyer, S., Anbar, A.D., 2011b. Uranium
759 isotope fractionation during adsorption to Mn-oxyhydroxides. Environmental
760 Science and Technology 45, 1370-1375.
761 Chen, J.H., Lawrence Edwards, R., Wasserburg, G.J., 1986. ^{238}U, ^{234}U and ^{232}Th in
762 seawater. Earth and Planetary Science Letters 80, 241-251.
763 Chen, K., Walker, R.J., Rudnick, R.L., Gao, S., Gaschnig, R.M., Puchtel, I.S. Tang, M.,
764 Hu, Z.-C., 2016. Platinum-group element abundances and Re-Os isotopic
765 systematics of the upper continental crust through time: Evidence from glacial
766 diamictites. Geochimica et Cosmochimica Acta 191, 1-16.
767 Chen, X., Romaniello, S.J., Herrmann, A.D., Wasylenki, L.E., Anbar, A.D., 2016.
768 Uranium isotope fractionation during coprecipitation with aragonite and calcite.
769 Geochimica et Cosmochimica Acta 188, 189-207.
770 Cole, D.B., Reinhard, C.T., Wang, X., Gueguen, B., Halverson, G.P., Gibson, T.,
771 Hodgskiss, M.S.W., McKenzie, N.R., Lyons, T.W., Planavsky, N.J., 2016. A
772 shale-hosted Cr isotope record of low atmospheric oxygen during the Proterozoic.
773 Geology 44, 555-558.

774 Cooke, D.R., Bull, S.W., Donovan, S., Rogers, J.R., 1998. K-metasomatism and base
775 metal depletion in volcanic rocks from the McArthur Basin, Northern
776 Territory—implications for base metal mineralization. Economic Geology 93,
777 1237-1263.
778 Cox, G.M., Jarrett, A., Edwards, D., Crockford, P.W., Halverson, G.P., Collins, A.S.,
779 Poirier, A., Li, Z.X., 2016. Basin redox and primary productivity within the
780 Mesoproterozoic Roper Seaway. Chemical Geology 440, 101-114.
781 Crick, I.H., Boreham, C.J., Cook, A.C., Powell, T.G., 1988. Petroleum geology and
782 geochemistry of Middle Proterozoic McArthur Basin, northern Australia II:
783 assessment of source rock potential. American Association of Petroleum Geologists
784 Bulletin 72, 1495-1514.
785 Crowe, S.A., Dossing, L.N., Beukes, N.J., Bau, M., Kruger, S.J., Frei, R., Canfield, D.E.,
786 2013. Atmospheric oxygenation three billion years ago. Nature 501, 535-538.
787 Dahl, T.W., Canfield, D.E., Rosing, M.T., Frei, R.E., Gordon, G.W., Knoll, A.H., Anbar,
788 A.D., 2011. Molybdenum evidence for expansive sulfidic water masses in ~750 Ma
789 oceans. Earth and Planetary Science Letters 311, 264-274.
790 Dahl, T.W., Boyle, R.A., Canfield, D.E., Connelly, J.N., Gill, B.C., Lenton, T.M.,
791 Bizzaro, M., 2014. Uranium isotopes distinguish two geochemically distinct stages
792 during the later Cambrian SPICE event. Earth and Planetary Science Letters 401,
793 313-326.

794 Daines, S.J., Mills, B.J.W., Lenton, T.M., 2017. Atmospheric oxygen regulation at low
795 Proterozoic levels by incomplete oxidative weathering of sedimentary organic
796 carbon. Nature Communications. 8:14379; DOI: 10.1038/ncomms14379, 1-11.
797 D'Arcy, J., Babechuk, M.G., Dossing, L.N., Gaucher, C., Frei R., 2016. Processes
798 controlling the chromium isotopic composition of river water: constraints from
799 basaltic river catchments. Geochimica et Cosmochimica Acta 186, 296-315.
800 Dhuime, B., Wuestefeld, A., Hawkesworth, C.J. 2015. Emergence of modern continental
801 crust about 3 billion years ago. Nature Geoscience 8, 552-555.
802 Donnelly, T.H., Jackson, M.J., 1988. Sedimentology and geochemistry of a
803 Mid-Proterozoic lacustrine unit from northern Australia. Sedimentary Geology 58,
804 145-169.
805 Dunk, R.M., Mills, R.A., Jenkins, W.J., 2002. A reevaluation of the oceanic uranium
806 budget for the Holocene. Chemical Geology 190, 45-67.
807 Elrick, M., Polyak, V., Algeo, T.J., Romaniello, S., Asmerom, Y., Herrmann, A.D.,
808 Anbar, A.D., Zhao, L., Chen Z.-Q., 2017. Global-ocean redox variation during the
809 middle-late Permian through Early Triassic based on uranium isotope and Th/U
810 trends of marine carbonates. Geology 45, 163-166.
811 Esser, B.K., Turekian, K.K., 1993. The osmium isotopic composition of the continental
812 crust. Geochimica et Cosmochimica Acta 57, 3093-3104.

813 Flannery, E.N., George, S.C., 2014. Assessing the syngeneity and indigeneity of
814 hydrocarbons in the ~1.4 Ga Velkerri Formation, McArthur Basin, using slice
815 experiments. Organic Geochemistry 77, 115-125.
816 Garven, G., Bull, S.W., Large, R.R., 2001. Hydrothermal fluid flow models of stratiform
817 ore genesis in the McArthur Basin, Northern Territory, Australia. Geofluids 1,
818 289-311.
819 George, S.C., Ahmed, M., 2002. Use of aromatic compound distributions to evaluate
820 organic maturity of the Proterozoic Middle Velkerri Formation, McArthur Basin,
821 Australia, in: Keep, M., Moss S.J. (Eds.), The Sedimentary Basins of Western
822 Australia 3. Proceedings of the Petroleum Exploration Society of Australia
823 Symposium, pp. 253-270.
824 Gilleaudeau, G.J., Frei, R., Kaufman, A.J., Kah, L.C., Azmy, K., Bartley, J.K.,
825 Chernyavskiy, P., Knoll, A.H., 2016. Oxygenation of the mid-Proterozoic
826 atmosphere: clues from chromium isotopes in carbonates. Geochemical Perspectives
827 Letters 2, 178-187.
828 Goto, K.T., Anbar, A.D., Gordon, G.W., Romaniello, S.J., Shimoda, G., Takaya, Y.,
829 Tokumaru, A., Nozaki, T., Suzuki, K., Machida, S., Hanyu, T., Usui, A., 2014.
830 Uranium isotope systematics of ferromanganese crusts in the Pacific Ocean:
831 Implications for the marine $^{238}U/^{235}U$ isotope system. Geochimica et Cosmochimica
832 Acta 146, 43-58.

833 Gueguen, B., Reinhard, C.T., Algeo, T.J., Peterson, L.C., Nielsen, S.G., Wang, X., Rowe,
834 H., Planavsky, N.J., 2016. The chromium isotope composition of reducing and oxic
835 marine sediments. Geochimica et Cosmochimica Acta 184, 1-19.
836 Hastings, D.W., Emerson, S.R., Mix, A.C., 1996. Vanadium in foraminiferal calcite as a
837 tracer for changes in the areal extent of reducing sediments. Paleoceanography 11,
838 665-678.
839 Hattori, Y., Suzuki, K., Honda, M., Shimizu, H., 2003. Re–Os isotope systematics of the
840 Taklimakan Desert sands, moraines and river sediments around the Taklimakan
841 Desert, and of Tibetan soils. Geochimica et Cosmochimica Acta 67, 1203-1213.
842 Holmden, C., Amini, M., Francois, R., 2015. Uranium isotope fractionation in Saanich
843 Inlet: A modern analog study of a paleoredox tracer. Geochimica et Cosmochimica
844 Acta 153, 202-215.
845 Idnurm, M., 2000. Towards a high resolution Late Palaeoproterozoic – earliest
846 Mesoproterozoic apparent polar wander path for northern Australia. Australian
847 Journal of Earth Sciences 47, 405-429.
848 Idnurm, M., Giddings, J.W., Plumb, K.A., 1995. Apparent polar wander and reversal
849 stratigraphy of the Palaeo-Mesoproterozoic southeastern McArthur Basin, Australia.
850 Precambrian Research 72, 1-41.
851 Jackson, M.J., 1985. Mid-Proterozoic dolomitic varves and microcycles from the
852 McArthur Basin, northern Australia. Sedimentary Geology 44, 301-326.

853 Jackson, M.J., Raiswell, R., 1991. Sedimentology and carbon-sulphur geochemistry of
854 the Velkerri Formation, a mid-Proterozoic potential oil source in northern Australia.
855 Precambrian Research 54, 81-108.
856 Jackson, M.J., Scott, D.L., Rawlings, D.J., 2000. Stratigraphic framework for the
857 Leichhardt and Calvert Superbasins: review and correlations of the pre-1700 Ma
858 successions between Mt Isa and McArthur River. Australian Journal of Earth
859 Sciences 47, 381-403.
860 Jackson, M.J., Sweet, I.P., Page, R.W., Bradshaw, B.E., 1999. The South Nicholson and
861 Roper Groups: evidence for the early Mesoproterozoic Roper Superbasin, in:
862 Bradshaw, B.E., Scott, D.L. (Eds.), Integrated Basin Analysis of the Isa Superbasin
863 using Seismic, Well-log, and Geopotential Data: An Evaluation of the Economic
864 Potential of the Northern Lawn Hill Platform. Australian Geological Survey
865 Organisation Record 1999/19, Canberra, Australia, unpaginated.
866 Johnston, D.T., Farquhar, J., Summons, R.E., Shen, Y., Kaufman, A.J., Masterson, A.L.,
867 Canfield, D.E., 2008. Sulfur isotope biogeochemistry of the Proterozoic McArthur
868 Basin. Geochimica et Cosmochimica Acta 72, 4278-4290.
869 Kendall, B., Brennecka, G.A., Weyer, S., Anbar, A.D., 2013. Uranium isotope
870 fractionation suggests oxidative uranium mobilization at 2.50 Ga. Chemical
871 Geology 362, 105-114.

872 Kendall, B., Creaser, R.A., Gordon, G.W., Anbar, A.D., 2009. Re-Os and Mo isotope
873 systematics of black shales from the Middle Proterozoic Velkerri and Wollogorang
874 Formations, McArthur Basin, northern Australia. Geochimica et Cosmochimica
875 Acta 73, 2534-2558.
876 Kendall, B., Komiya, T., Lyons, T.W., Bates, S.M., Gordon, G.W., Romaniello, S.J., Jiang,
877 G., Creaser, R.A., Xiao, S., McFadden, K., Sawaki, Y., Tahata, M., Shu, D., Han, J.,
878 Li, Y., Chu, X., Anbar, A.D., 2015. Uranium and molybdenum isotope evidence for
879 an episode of widespread ocean oxygenation during the late Ediacaran
880 Period. Geochimica et Cosmochimica Acta 156, 173-193.
881 Kendall, B.*, Dahl, T.W.*, Anbar, A.D., 2017. Good golly, why moly? The stable isotope
882 geochemistry of molybdenum. Reviews in Mineralogy and Geochemistry 82,
883 683-732. *These authors contributed equally.
884 Koehler, M.C., Stüeken, E.E., Kipp, M.A., Buick, R., Knoll, A.H., 2017. Spatial and
885 temporal trends in Precambrian nitrogen cycling: A Mesoproterozoic offshore nitrate
886 minimum. Geochimica et Cosmochimica Acta 198, 315-337.
887 Ku, T.L., Knauss, K., Mathieu, G.G., 1977. Uranium in the open ocean: concentration
888 and isotopic composition. Deep Sea Research 24, 1005-1017.
889 Langmuir, D., 1978. Uranium solution-mineral equilibria at low temperatures with
890 applications to sedimentary ore deposits. Geochimica et Cosmochimica Acta 42,
891 547-569.

892 Large, R.R., Bull, S.W., Cooke, D.R., McGoldrick, P.J., 1998. A genetic model for the
893 HYC Deposit, Australia; based on regional sedimentology, geochemistry, and
894 sulfide-sediment relationships. Economic Geology 93, 1345-1368.
895 Large, R.R., Bull, S.W., Winefield, P.R., 2001. Carbon and oxygen isotope halo in
896 carbonates related to the McArthur River (HYC) Zn–Pb–Ag deposit, North
897 Australia: implications for sedimentation, ore genesis, and mineral exploration.
898 Economic Geology 96, 1567-1593.
899 Lau, K.V., Maher, K., Altiner, D., Kelley, B.M., Kump, L.R., Lehrmann, D.J., Silva-
900 Tamayo, J.C., Weaver, K.L., Yu, M., Payne, J.L., 2016. Marine anoxia and delayed
901 Earth system recovery after the end-Permian extinction. Proceedings of the National
902 Academy of Sciences U.S.A. 113, 2360-2365.
903 Lau, K.V., Macdonald, F.A., Maher, K., Payne, J.L., 2017. Uranium isotope evidence for
904 temporary ocean oxygenation in the aftermath of the Sturtian snowball Earth. Earth
905 and Planetary Science Letters 458, 282-292.
906 Liu, X.M., Kah, L.C., Knoll, A.H., Cui, H., Kaufman, A.J., Shahar, A., Hazen, R.M.,
907 2016. Tracing Earth's O_2 evolution using Zn/Fe ratios in marine
908 carbonates. Geochemical Perspectives Letters 2, 24-34.
909 Logan, G.A., Hinman, M.C., Walter, M.R., Summons, R.E., 2001. Biogeochemistry of
910 the 1640 Ma McArthur River (HYC) lead–zinc ore and host sediments, Northern
911 territories, Australia. Geochimica et Cosmochimica Acta 65, 2317-2336.

912 Lu, X., Kendall, B., Stein, H.J., Li, C., Hannah, J.L., Gordon, G.W., Ebbestad, J.O.R., in
913 press. Marine redox conditions during deposition of late Ordovician and early
914 Silurian organic-rich mudrocks in the Siljan ring district, central Sweden. Chemical
915 Geology 457, 75-94.
916 Luo, G., Ono, S., Huang, J., Algeo, T.J., Li, C., Zhou, L., Robinson, A., Lyons, T.W., Xie,
917 S., 2015. Decline in oceanic sulfate levels during the early Mesoproterozoic.
918 Precambrian Research 258, 36-47.
919 Lyons, T.W., Reinhard, C.T., Planavsky, N.J. 2014. The rise of oxygen in Earth's early
920 ocean and atmosphere. Nature 506, 307-315.
921 Lyons, T.W., Severmann S., 2006. A critical look at iron paleoredox proxies: new
922 insights from modern euxinic marine basins. Geochimica et Cosmochimica Acta 70,
923 5698-5722.
924 McLennan, S.M., 2001. Relationships between the trace element composition of
925 sedimentary rocks and upper continental crust. Geochemistry Geophysics
926 Geosystems 2, Paper No. 2000GC000109.
927 Montoya-Pino, C., Weyer, S., Anbar, A.D., Pross, J., Oschmann, W., van de
928 Schootbrugge, B., Arz, H.W., 2010. Global enhancement of ocean anoxia during
929 Oceanic Anoxic Event 2: a quantitative approach using U isotopes. Geology 38,
930 315-318.

931 Morford, J.L., Emerson, S.R., 1999. The geochemistry of redox sensitive trace metals in
932 sediments. Geochimica et Cosmochimica Acta 63, 1735-1750.
933 Morford, J.L., Emerson, S.R., Breckel, E.J., Kim, S.H., 2005. Diagenesis of oxyanions (V,
934 U, Re, and Mo) in pore waters and sediments from a continental margin.
935 Geochimica et Cosmochimica Acta 69, 5021-5032.
936 Mukherjee, I., Large, R.R., 2016. Pyrite trace element chemistry of the Velkerri
937 Formation, Roper Group, McArthur Basin: Evidence for atmospheric oxygenation
938 during the Boring Billion. Precambrian Research 281, 13-26.
939 Myers, J.S., Shaw, R.D., Tyler, I.M., 1996. Tectonic evolution of Proterozoic Australia.
940 Tectonics 15, 1431-1446.
941 Nägler, T.F., Anbar, A.D., Archer, C., Goldberg, T., Gordon, G.W., Greber, N.D., Siebert,
942 C., Sohrin, Y., Vance, D., 2014. Proposal for an international molybdenum isotope
943 measurement standard and data representation. Geostandards and Geoanalytical
944 Research 38, 149-151.
945 Neubert, N., Nägler, T.F., Böttcher, M.E., 2008. Sulfidity controls molybdenum isotope
946 fractionation into euxinic sediments: evidence from the modern Black Sea.
947 Geochimica et Cosmochimica Acta 36, 775-778.
948 Noordmann, J., Weyer, S., Georg, R.B., Jons, S., Sharma, M., 2016. $^{238}U/^{235}U$ isotope
949 ratios of crustal material, rivers and products of hydrothermal alteration: new

insights on the oceanic U isotope mass balance. Isotopes in Environmental and Health Studies 52, 141-163.

Noordmann, J., Weyer, S., Montoya-Pino, C., Dellwig, O., Neubert, N., Eckert, S., Paetzel, M., Böttcher, M.E. 2015. Uranium and molybdenum isotope systematics in modern euxinic basins: Case studies from the central Baltic Sea and the Kyllaren fjord (Norway). Chemical Geology 396, 182-195.

Page, R.W., Jackson, M.J., Krassay, A.A., 2000. Constraining sequence stratigraphy in north Australian basins: SHRIMP U–Pb zircon geochronology between Mt Isa and McArthur River. Australian Journal of Earth Sciences 47, 431-459.

Partin, C.A., Bekker, A., Planavsky, N.J., Scott, C.T., Gill, B.C., Li, C., Podkovyrov, V., Maslov, A., Konhauser, K.O., Lalonde, S.V., Love, G.D., Poulton, S.W., Lyons, T.W., 2013. Large-scale fluctuations in Precambrian atmospheric and oceanic oxygen levels from the record of U in shales. Earth and Planetary Science Letters, 369-370, 284-293.

Paulukat, C., Gilleaudeau, G.J., Chernyavskiy, P., Frei, R., 2016. The Cr-isotope signature of surface seawater – a global perspective. Chemical Geology 444, 101-109.

Pawlowska, M.M., Butterfield, N.J., Brocks, J.J., 2013. Lipid taphonomy in the Proterozoic and the effect of microbial mats on biomarker preservation. Geology 41, 103-106.

970 Peucker-Ehrenbrink B., Jahn B., 2001. Rhenium-osmium isotope systematics and
971 platinum group element concentrations: Loess and the upper continental crust.
972 Geochemistry Geophysics Geosystems 2, 2001GC000172.
973 Planavsky, N.J., Cole, D.B., Reinhard, C.T., Diamond, C., Love, G.D., Luo, G., Zhang,
974 S., Konhauser, K.O., Lyons, T.W., 2016. No evidence for high atmospheric oxygen
975 levels 1,400 million years ago. Proceedings of the National Academy of Sciences
976 U.S.A. 113, E2550-E2551.
977 Planavsky, N.J., McGoldrick, P., Scott, C.T., Li, C., Reinhard, C.T., Kelly, A.E., Chu, X.,
978 Bekker, A., Love, G.D., Lyons, T.W., 2011. Widespread iron-rich conditions in the
979 mid-Proterozoic ocean. Nature 477, 448-451.
980 Planavsky, N.J., Reinhard, C.T., Wang, X., Thomson, D., McGoldrick, P., Rainbird, R.H.,
981 Johnson, T., Fischer, W.W., Lyons, T.W., 2014. Low Mid-Proterozoic atmospheric
982 oxygen levels and the delayed rise of animals. Science 346, 635-638.
983 Poulton, S.W., Canfield, D.E., 2011. Ferruginous conditions: a dominant feature of the
984 ocean through Earth's history. Elements 7, 107-112.
985 Raiswell, R., Buckley, F., Berner, R.A., Anderson, T.F., 1988. Degree of pyritization of
986 iron as a paleoenvironmental indicator of bottom-water oxygenation. Journal of
987 Sedimentary Petrology 58, 812-819.
988 Raiswell, R., Canfield, D.E., 1998. Sources of iron for pyrite formation in marine
989 sediments. American Journal of Science 298, 219-245.

990 Rawlings, D.J., Korsch, R.J., Goleby, B.R., Gibson, G.M., Johnstone, D.W., Barlow, M.,
991 2004. The 2002 southern McArthur Basin seismic reflection survey. Geoscience
992 Australia, Canberra.
993 Reinhard, C.T., Planavsky, N.J., Robbins, L.J., Partin, C.A., Gill, B.C., Lalonde, S.V.,
994 Bekker, A., Konhauser, K.O., Lyons, T.W., 2013. Proterozoic ocean redox and
995 biogeochemical stasis. Proceedings of the National Academy of Sciences U.S.A.
996 110, 5357-5362.
997 Reinhard, C.T., Planavsky, N.J., Olson, S.L., Lyons, T.W., Erwin, D.H., 2016. Earth's
998 oxygen cycle and the evolution of animal life. Proceedings of the National Academy
999 of Sciences U.S.A. 113, 8933-8938.
1000 Rolison, J.M., Stirling, C.H., Middag, R., Rijkenberg, M.J.A., 2017. Uranium stable
1001 isotope fractionation in the Black Sea: Modern calibration of the $^{238}U/^{235}U$
1002 paleo-redox proxy. Geochimica et Cosmochimica Acta 203, 69-88.
1003 Romaniello, S.J., Herrmann, A.D., Anbar, A.D., 2013. Uranium concentrations and
1004 $^{238}U/^{235}U$ isotope ratios in modern carbonates from the Bahamas: assessing a novel
1005 paleoredox proxy. Chemical Geology 362, 305-316.
1006 Scheiderich, K., Amini, M., Holmden, C., Francois, R., 2015. Global variability of
1007 chromium isotopes in seawater demonstrated by Pacific, Atlantic, and Arctic Ocean
1008 samples. Earth and Planetary Science Letters 423, 87-97.

1009 Schoenberg, R., Zink, S., Staubwasser, M., von Blanckenberg, F., 2008. The stable Cr
1010 isotope inventory of solid Earth reservoirs determined by double spike MC-ICP-MS.
1011 Chemical Geology 249, 294-306.
1012 Scott, C., Lyons, T.W., 2012. Contrasting molybdenum cycling and isotopic properties in
1013 euxinic versus non-euxinic sediments and sedimentary rocks: Refining the
1014 paleoproxies. Chemical Geology 324-325, 19-27.
1015 Scott, C., Lyons, T.W., Bekker, A., Shen, Y., Poulton, S.W., Chu X., Anbar, A.D., 2008.
1016 Tracing the stepwise oxygenation of the Proterozoic ocean. Nature 452, 456-459.
1017 Scott, C., Planavsky, N.J., Dupont, C.L., Kendall, B., Gill, B.C., Robbins, L.J., Husband,
1018 K.F., Arnold, G.L., Wing, B.A., Poulton, S.W., Bekker, A., Anbar, A.D., Konhauser,
1019 K.O., Lyons, T.W., 2013. Bioavailability of zinc in marine systems through
1020 time. Nature Geoscience 6, 125-128.
1021 Scott, D.L., Rawlings, D.J., Page, R.W., Tarlowski, C.Z., Idnurm, M., Jackson, M.J.,
1022 Southgate, P.N., 2000. Basement framework and geodynamic evolution of the
1023 Palaeoproterozoic superbasins of north-central Australia: an integrated review of
1024 geochemical, geochronological and geophysical data. Australian Journal of Earth
1025 Sciences 47, 341-380.
1026 Shen, Y., Canfield, D.E., Knoll A.H., 2002. Middle Proterozoic ocean chemistry:
1027 evidence from the McArthur Basin, northern Australia. American Journal of Science
1028 302, 81-109.

1029 Shen, Y., Knoll, A.H., Walter, M.R., 2003. Evidence for low sulphate and anoxia in a
1030 mid-Proterozoic marine basin. Nature 423, 632-635.
1031 Southgate, P.N., Bradshaw, B.E., Domagala, J., Jackson, M.J., Idnurm, M., Krassay, A.A.,
1032 Page, R.W., Sami, T.T., Scott, D.L., Lindsay, J.F., McConachie, B.A., Tarlowski, C.,
1033 2000. Chronostratigraphic basin framework for Palaeoproterozoic rocks (1730-1575
1034 Ma) in northern Australia and implications for base-metal mineralization. Australian
1035 Journal of Earth Sciences 47, 461-483.
1036 Sperling, E.A., Rooney, A.D., Hays, L., Sergeev, V.N., Vorob'eva, N.G., Sergeeva, N.D.,
1037 Vorob'eva, N.G., Sergeeva, N.D., Selby, D., Johnston, D.T. and Knoll, A.H., 2014.
1038 Redox heterogeneity of subsurface waters in the Mesoproterozoic ocean.
1039 Geobiology 12, 373-386.
1040 Sperling, E.A., Wolock, C.J., Morgan, A.S., Gill, B.C., Kunzmann, M., Halverson, G.P.,
1041 Macdonald, F.A., Knoll, A.H., Johnston, D.T., 2015. Statistical analysis of iron
1042 geochemical data suggests limited late Proterozoic oxygenation. Nature 523,
1043 451-454.
1044 Spinks, S.C., Schmid, S., Pagés, A., Bluett, J., 2016. Evidence for SEDEX-style
1045 mineralization in the 1.7 Ga Tawallah Group, McArthur Basin, Australia. Ore
1046 Geology Reviews 76, 122-139.
1047 Stirling, C.H., Andersen, M.B., Potter, E.K., Halliday, A.H., 2007. Low-temperature
1048 isotopic fractionation of uranium. Earth and Planetary Science Letters 264, 208-225.

1049 Stirling, C.H., Andersen, M.B., Warthmann, R., Halliday, A.N., 2015. Isotope
1050 fractionation of ^{238}U and ^{235}U during biologically-mediated uranium reduction.
1051 Geochimica et Cosmochimica Acta 163, 200-218.
1052 Stylo, M., Neubert, N., Wang, Y., Monga, N., Romaniello, S.J., Weyer, S.,
1053 Bernier-Latmani, R., 2015. Uranium isotopes fingerprint biotic reduction.
1054 Proceedings of the National Academy of Sciences U.S.A. 112, 5619-5624.
1055 Summons, R.E., Powell, T.G., Boreham, C.J., 1988. Petroleum geology and
1056 geochemistry of the Middle Proterozoic McArthur Basin, northern Australia: III.
1057 Composition of extractable hydrocarbons. Geochimica et Cosmochimica Acta 52,
1058 1747-1763.
1059 Summons, R.E., Taylor, D., Boreham, C.J., 1994. Geochemical tools for evaluating
1060 petroleum generation in Middle Proterozoic sediments of the McArthur Basin,
1061 Northern Territory, Australia. Australian Petroleum Production and Exploration
1062 Association Journal 34, 692-706.
1063 Tang, D., Shi, X., Wang, X., Jiang, G., 2016. Extremely low oxygen concentration in
1064 mid-Proterozoic shallow seawaters. Precambrian Research 276, 145-157.
1065 Taylor, D., Kontorovich, A.E., Larichev, A.I., Glikson, M., 1994. Petroleum source rocks
1066 in the Roper Group of the McArthur Basin: Source characterization and maturity
1067 determinations using physical and chemical methods. Australian Petroleum
1068 Production and Exploration Association Journal 34, 279-296.

1069 Telus, M., Dauphas, N., Moynier, F., Tissot, F.L.H., Teng, F.-Z., Nabelek, P.I., Craddock,
1070 P.R., Groat, L.A., 2012. Iron, zinc, magnesium and uranium isotopic fractionation
1071 during continental crust differentiation: the tale from migmatites, granitoids, and
1072 pegmatites. Geochimica et Cosmochimica Acta 97, 247-265.
1073 Tissot, F.L.H., Dauphas, N., 2015. Uranium isotopic compositions of the crust and ocean:
1074 Age corrections, U budget and global extent of modern anoxia. Geochimica et
1075 Cosmochimica Acta 167, 113-143.
1076 Tribovillard, N., Algeo, T.J., Lyons, T.W., Riboulleau, A., 2006. Trace metals as
1077 paleoredox and paleoproductivity proxies: An update. Chemical Geology 232,
1078 12-32.
1079 Veeh, H.H., 1967. Deposition of uranium from the ocean. Earth and Planetary Science
1080 Letters 3, 145-150.
1081 Volk, H., George, S.C., Dutkiewicz, A., Ridley, J., 2005. Characterisation of fluid
1082 inclusion oil in a Mid-Proterozoic sandstone and dolerite (Roper Superbasin,
1083 Australia). Chemical Geology 223, 109-135.
1084 Wang, X., Planavsky, N.J., Reinhard, C.T., Hein, J.R., Johnson, T.M., 2016. A Cenozoic
1085 seawater redox record derived from $^{238}U/^{235}U$ in ferromanganese crusts. American
1086 Journal of Science 316, 64-83.
1087 Warren, J.K., George, S.C., Hamilton, P.J., Tingate, P., 1998. Proterozoic source rocks:
1088 sedimentology and organic characteristics of the Velkerri Formation, Northern

Territory, Australia. American Association of Petroleum Geologists Bulletin 82, 442-463.

Weyer, S., Anbar, A.D., Gerdes, A., Gordon, G.W., Algeo, T.J., Boyle, E.A., 2008. Natural fractionation of $^{238}U/^{235}U$. Geochimica et Cosmochimica Acta 72, 345-359.

Williford, K.H., Grice, K., Logan, G.A., Chen, J., Huston, D., 2011. The molecular and isotopic effects of hydrothermal alteration of organic matter in the Paleoproterozoic McArthur River Pb/Zn/Ag ore deposit. Earth and Planetary Science Letters 301, 382-392.

Wu, W., Wang, X., Reinhard, C.T., Planavsky, N.J., 2017. Chromium isotope systematics in the Connecticut River. Chemical Geology 456, 98-111.

Zhang, S., Wang, X., Wang, H., Bjerrum, C.J., Hammarlund, E.U., Costa, M.M., Connelly, J.N., Zhang, B., Su, J., Canfield, D.E., 2016. Sufficient oxygen for animal respiration 1,400 million years ago. Proceedings of the National Academy of Sciences U.S.A. 113, 1731-1736.

Figure Captions

Fig. 1. Regional geological map of the McArthur Basin in Northern Australia. The location of the two drill holes Urapunga-4 (Velkerri Formation) and Mount Young 2 (Wollogorang Formation) are shown. Modified from Volk et al. (2005), Kendall et al.

(2009), and Mukherjee and Large (2016).

Fig. 2. Lithostratigraphy of the Velkerri Formation in drill hole Urapunga-4. Re-Os depositional ages from Kendall et al. (2009). Modified from Mukherjee and Large (2016).

Fig. 3. Lithostratigraphy of the Wollogorang Formation in drill hole Mount Young 2. Modified from Donnelly and Jackson (1988) and Kendall et al. (2009). U–Pb zircon ages of tuffaceous beds are from Page et al. (2000).

Fig. 4. Geochemical profiles for the Velkerri Formation (drill hole Urapunga-4). Lithostratigraphic column is modified from Mukherjee and Large (2016). For the geochemical profiles spanning the entire Velkerri Formation (blue circles), the TOC, S, Mo, and U data are from Mukherjee and Large (2016); the δ^{98}Mo data are from Arnold et al. (2004); and the Fe_{HR}/Fe_T and DOP data are from Shen et al. (2003). The red circles denote data from Kendall et al. (2009) and this study. The blue dashed line at Fe_{HR}/Fe_T = 0.38 and the red dashed line at DOP = 0.45 represent the threshold above which local bottom waters were likely anoxic. DOP values above 0.75 likely represent euxinic conditions (Raiswell et al., 1988; Raiswell and Canfield, 1998; Lyons and Severmann, 2006). No TOC or Mo isotope data exist for the lower Velkerri interval (325.71-326.69

m).

Fig. 5. $\delta^{238}U$ versus U_{EF} for the Velkerri Formation. Upper Velkerri and Lower Velkerri refers to samples from 136.98-137.89 m and 325.71-326.69 m in Urapunga-4, respectively.

Fig. 6. Geochemical profiles for the Wollogorang Formation (drill hole Mount Young 2). Lithostratigraphic column is modified from Donnelly and Jackson (1988) and Kendall et al. (2009). The DOP, Fe_T/Al, $\delta^{98}Mo$, and Mo EF data are from Kendall et al. (2009). The red squares denote data from 76.91-76.96 (dol) (shale material adjacent to a dolomite veinlet). The red dashed line denotes DOP = 0.45.

Fig. 7. $\delta^{238}U$ versus U_{EF} for the Wollogorang Formation. Shallow Wollogorang and Deep Wollogorang refers to samples from 74.27-75.53 m and 76.00-76.96 m in Mount Young 2, respectively.

Fig. 8. $\delta^{98}Mo$ versus $\delta^{238}U$ for the Wollogorang Formation and upper Velkerri Formation. Shallow Wollogorang and Deep Wollogorang refers to samples from 74.27-75.53 m and 76.00-76.96 m in Mount Young 2, respectively. Upper Velkerri refers to samples from 136.98-137.89 m in Urapunga-4.

Fig. 9. Results of U isotope mass balance modelling, showing $\delta^{238}U_{seawater}$ versus anoxic seafloor area, assuming a global U isotope fractionation factor of A) 0.60‰ and B) 0.85‰ between seawater and anoxic sediments. The $\delta^{238}U_{seawater}$ for the upper Velkerri Formation (blue) is –0.47‰ to –0.72‰, whereas $\delta^{238}U_{seawater}$ for the lower Velkerri Formation (purple) is –0.68‰ to –0.93‰ (assuming local fractionation factors of 0.60-0.85‰ during U removal from seawater to the Velkerri sediments). Dashed line represents modern $\delta^{238}U_{seawater}$ (= –0.39‰).

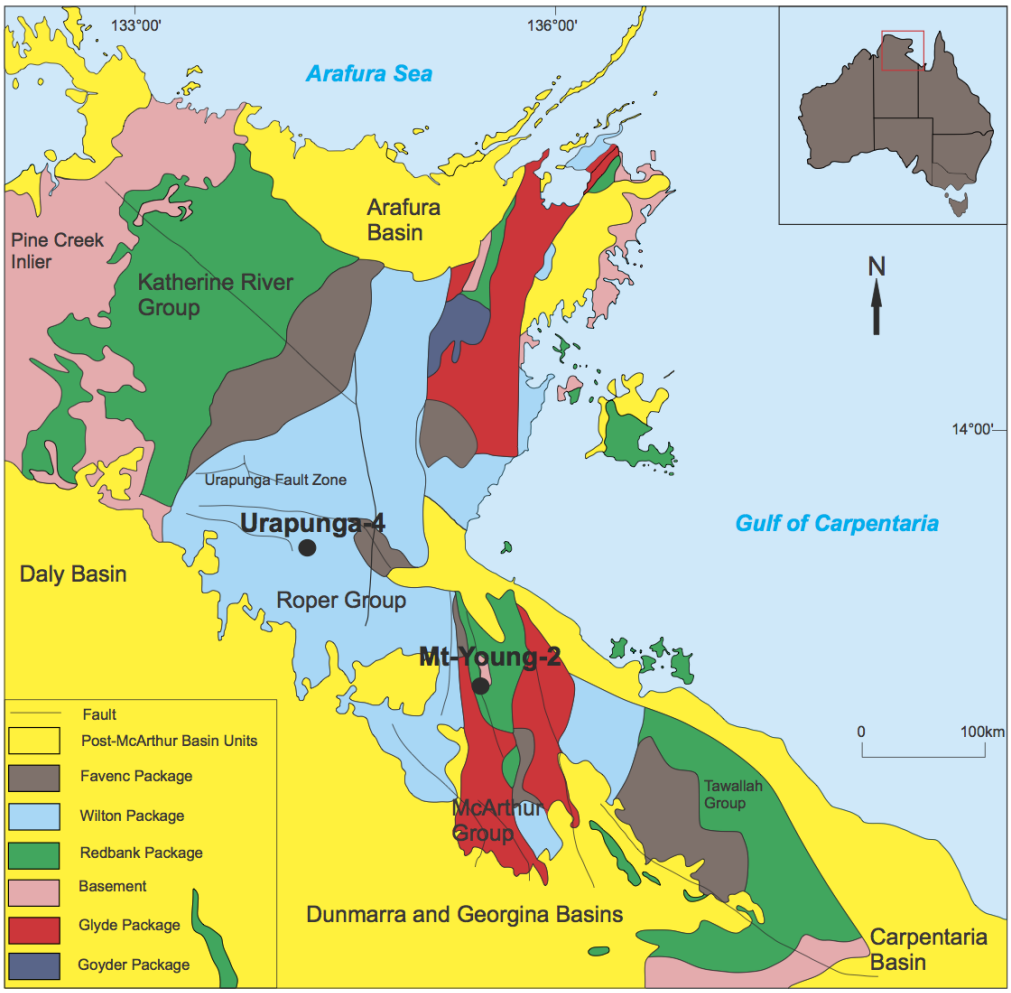

1158

1159

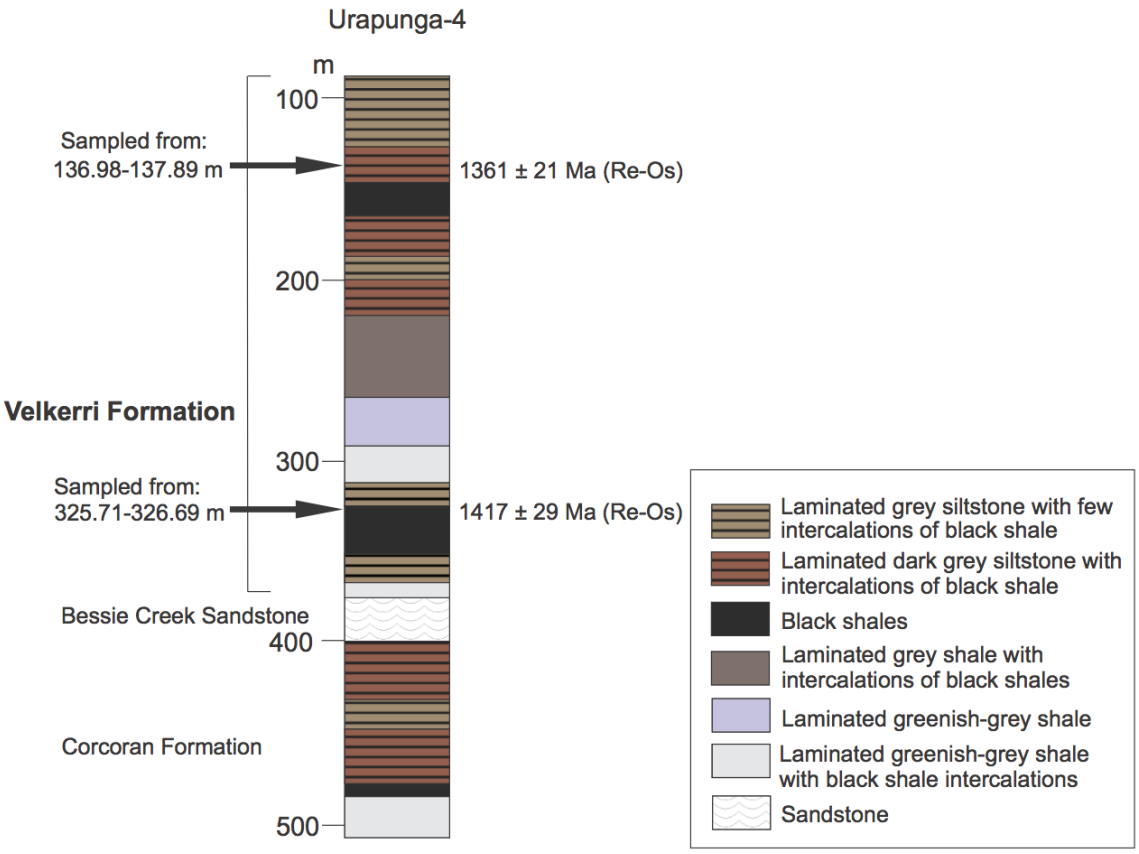

1160

1161

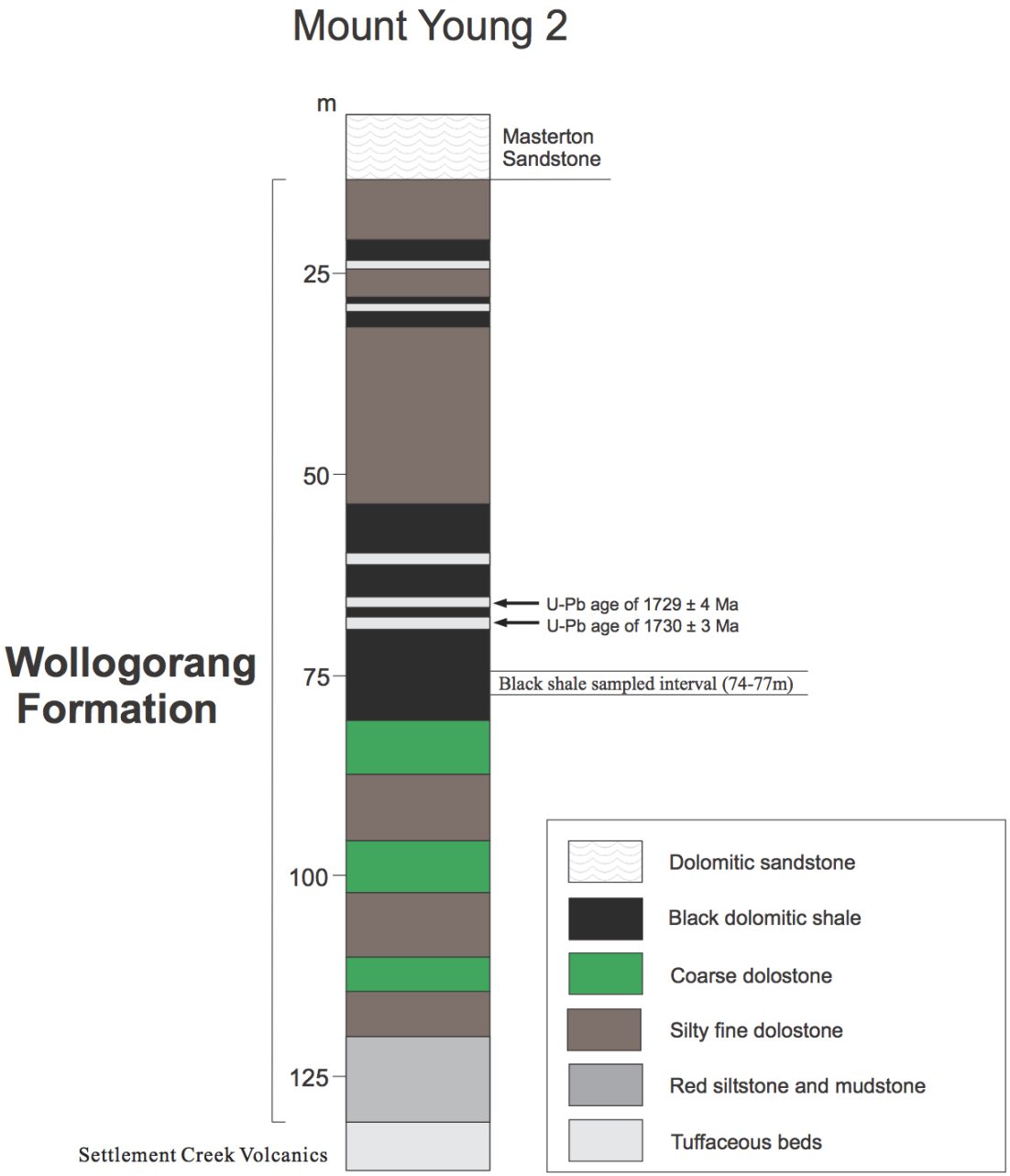

1162

1163

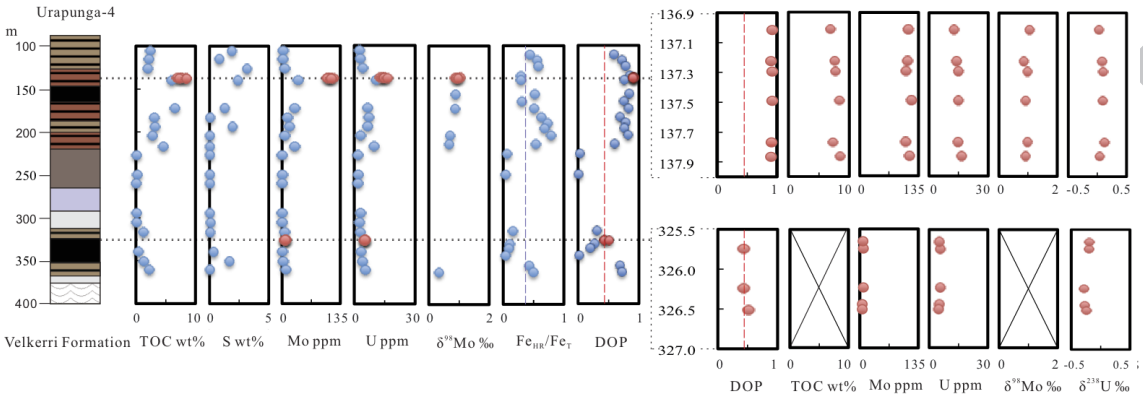

1164
1165

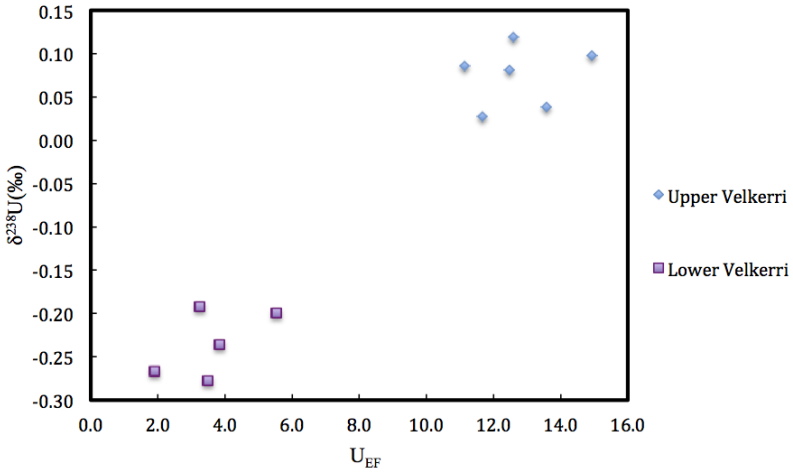

1166

1167

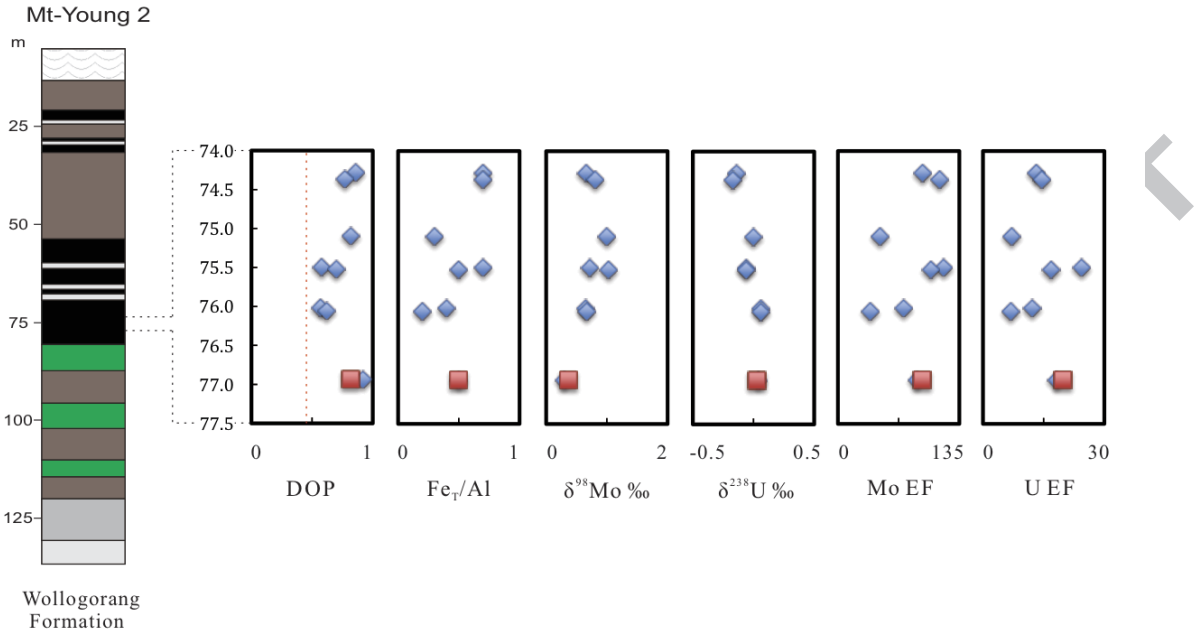

1168

1169

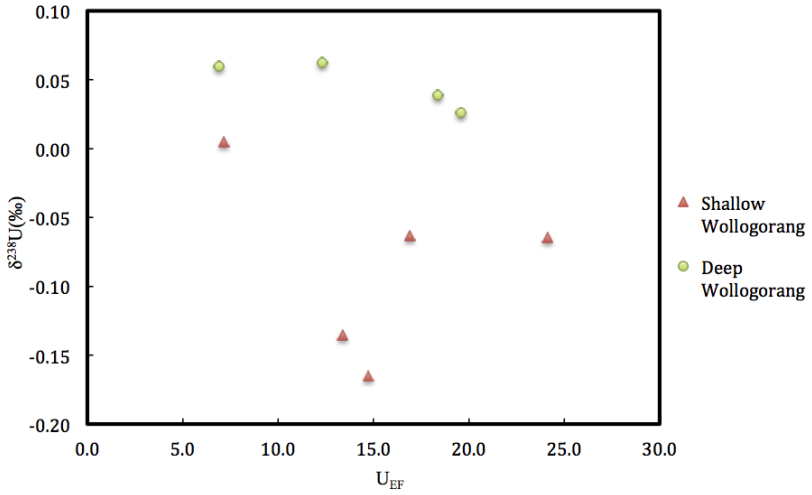

1170

1171

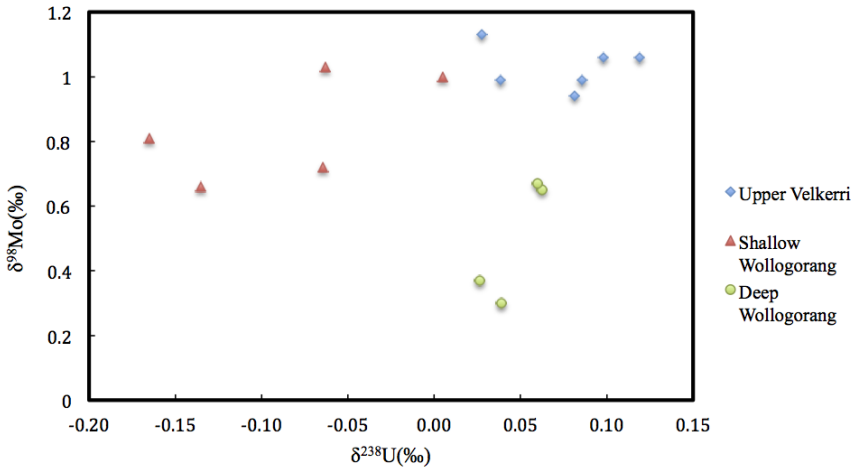

1172

1173

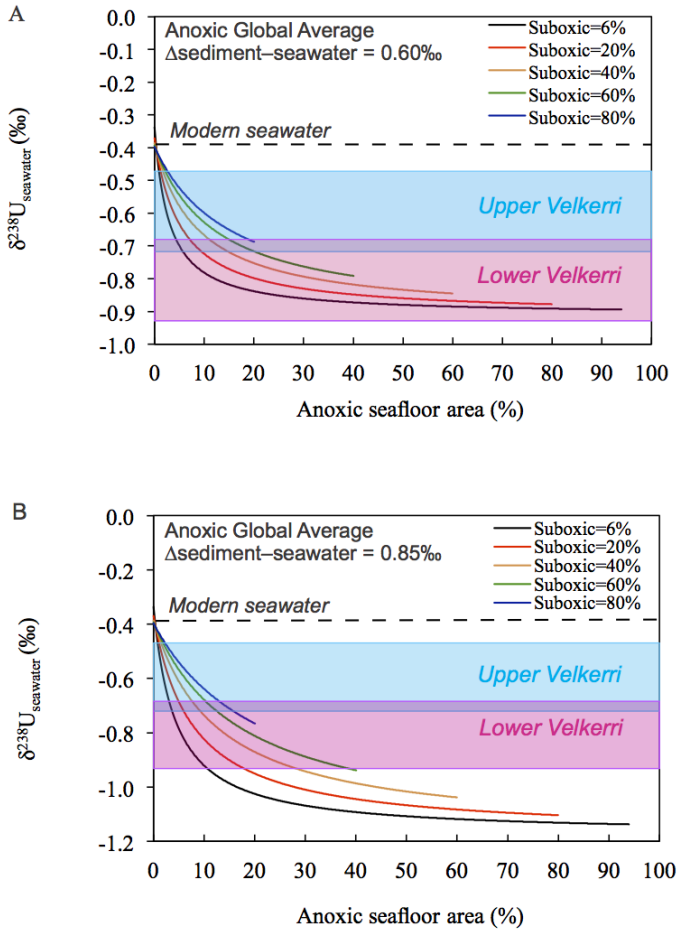

1174

1175

Table 1. Geochemical data for black shales from the Velkerri Formation and Wollogorang Formation.

Core depth[a] (m)	Al (wt%)	Fe (wt%)	U (ppm)	Mo (ppm)	U_{EF}[b]	Mo_{EF}[b]	δ^{98}Mo (‰)[c]	2SD Measured	2SD Reported[d]	δ^{238}U (‰)	2SD Measured	2SD Reported[e]	n	Fe/Al	DOP[f]
Velkerri Formation (drillhole Urapunga-4)															
136.98-137.05	3.1	5.6	12.7	112	11.8	194	1.05	0.14	0.15	0.03	0.08	0.08	3	1.8	0.92
136.98-137.05 (rpt)			14.3							0.07	0.03	0.08	3		
137.19-137.26	3.2	5.1	13.9	110	12.5	184	0.86	0.10	0.15	0.08	0.02	0.08	3	1.6	0.90
137.26-137.33	2.9	5.3	14.8	106	14.7	196	0.98	0.06	0.15	0.10	0.07	0.08	3	1.8	0.92
137.46-137.52	3.8	5.4	14.8	119	11.2	168	0.91	0.11	0.15	0.09	0.03	0.08	3	1.4	0.92
137.75-137.79	3.3	5.6	14.7	105	12.8	171	0.98	0.15	0.15	0.12	0.08	0.08	3	1.7	0.91
137.84-137.89	3.5	5.2	16.5	114	13.5	175	0.91	0.09	0.15	0.04	0.02	0.08	3	1.5	0.90
137.84-137.			16.5							0.06	0.08	0.08	3		

89 (rpt)														
325.71-325.78	2.9	4.0	5.6	8.6	5.5	16				-0.20	0.03	0.08	3	1.4	0.43
326.20-326.28	4.6	3.3	5.6	8.8	3.5	10				-0.28	0.04	0.08	3	0.7	0.43
326.42-326.48	7.9	3.6	5.2	6.0	1.9	4.1				-0.27	0.10	0.10	3	0.5	
326.48-326.55	3.6	3.5	4.8	6.0	3.8	8.9				-0.24	0.07	0.08	3	1.0	0.51
326.48-326.55 (rpt)			4.8							-0.27	0.05	0.08	3		
326.62-326.69	4.6	4.2	5.2	7.5	3.2	8.7				-0.19	0.05	0.08	3	0.9	
Wollogorang Formation (drillhole Mount Young 2)															
74.27-74.29	3.3	2.4	15.2	58	13.2	94	0.66	0.11	0.15	-0.14	0.06	0.08	3	0.7	0.86
74.35-74.38	2.7	1.9	13.7	57	14.6	113	0.81	0.01	0.15	-0.17	0.06	0.08	3	0.7	0.77
75.08-75.11	4.7	1.3	11.7	41	7.1	47	1.00	0.07	0.15	0.00	0.06	0.08	3	0.3	0.82
75.48-75.51	2.6	1.8	22.1	57	24.4	118	0.72	0.12	0.15	-0.06	0.00	0.08	3	0.7	0.58
75.51-	2.9	1.5	17	56	1	1	1.0	0.18	0.18	-0.	0.02	0.08	3	0.	0.

75.53			.1		6.912	04	3			06			5	70
76.00-76.03	4.1	1.5	17.4	56	2.2	73	0.65	0.09	0.15	0.06	0.06	0.08	3	0.4	0.57
76.00-76.03 (rpt)			17.3							0.03	0.09	0.09	3		
76.03-76.08	7.7	1.7	18.6	52	6.918	36	0.67	0.07	0.15	0.06	0.09	0.09	3	0.2	0.62
76.91-76.96	3.4	1.6	21.6	56	8.219	88	0.30	0.11	0.15	0.04	0.05	0.08	3	0.5	0.92
76.91-76.96 (dol)	2.8	1.4	19.3	49	9.48	94	0.37	0.12	0.15	0.03	0.09	0.09	3	0.5	0.82

Note: U concentration and isotope data are from this study; Al, Fe, Mo, and DOP data are from Kendall et al. (2009).

[a]"rpt" = full powder replicate analysis; "dol" = shale material adjacent to dolomite veinlet.

[b]EF = enrichment factor = $(metal/Al)_{sample}$ / $(metal/Al)_{average\ upper\ crust}$. Upper crust data (Al = 8.04 wt%, U = 2.8 ppm, Mo = 1.5 ppm) are from McLennan (2001).

[c]Molybenum isotope data from Kendall et al. (2009) have been re-calculated relative to NIST SRM = 0.25‰.

[d]reported uncertainty for δ^{98}Mo is the 2SD of replicate measurements or 0.15‰, whichever is greater (Kendall et al., 2009).

1185 [e]reported uncertainty for $\delta^{238}U$ is the 2SD of replicate measurements or 0.08‰, whichever

1186 is greater.

1187 [f]DOP = degree of pyritization.

1188

Table 2. Authigenic U isotope composition and proportion of authigenic U in the Velkerri Formation and Wollogorang Formation.

Core depth[a] (m)	Al (wt %)	U (ppm)	δ^{238}U (‰)	2SD Measured	2SD[b] Reported	n	$\delta^{238}U_{auth}$[c] (‰)	f_{auth}[e] (%)	f_{det}[f] (%)	$\delta^{238}U_{auth}$[c] (‰)	f_{auth}[e] (%)	f_{det}[f] (%)
Velkerri Formation (drillhole Urapunga-4)							$\delta^{238}U_{det}$[d] = -0.3‰			$\delta^{238}U_{det}$[d] = -0.8‰		
136.98-137.05	3.1	12.7	0.03	0.08	0.08	3	0.06	91.4	8.6	0.11	91.4	8.6
137.19-137.26	3.2	13.9	0.08	0.02	0.08	3	0.11	92.0	8.0	0.16	92.0	8.0
137.26-137.33	2.9	14.8	0.10	0.07	0.08	3	0.13	93.3	6.7	0.16	93.3	6.7
137.46-137.52	3.8	14.8	0.09	0.03	0.08	3	0.12	91.0	9.0	0.17	91.0	9.0
137.75-137.79	3.3	14.7	0.12	0.08	0.08	3	0.16	92.1	7.9	0.20	92.1	7.9
137.84-137.89	3.5	16.5	0.04	0.02	0.08	3	0.07	92.6	7.4	0.11	92.6	7.4
325.71-325.78	2.9	5.6	-0.20	0.03	0.08	3	-0.18	81.9	18.1	-0.07	81.9	18.1
326.20-326.28	4.6	5.6	-0.28	0.04	0.08	3	-0.27	71.3	28.7	-0.07	71.3	28.7
326.42-326.48	7.9	5.2	-0.27	0.10	0.10	3	-0.23	47.4	52.6	0.33	47.4	52.6
326.48-326.55	3.6	4.8	-0.24	0.07	0.08	3	-0.21	73.9	26.1	-0.04	73.9	26.1
326.62-326.69	4.6	5.2	-0.19	0.05	0.08	3	-0.14	69.2	30.8	0.08	69.2	30.8
Wollogorang Formation (drillhole Mount Young 2)												
74.27-74.29	3.3	15.2	-0.14	0.06	0.08	3	-0.12	92.5	7.5	-0.08	92.5	7.5
74.35-74.38	2.7	13.7	-0.17	0.06	0.08	3	-0.16	93.2	6.8	-0.12	93.2	6.8
75.08-75.11	4.7	11.7	0.00	0.06	0.08	3	0.05	86.0	14.0	0.14	86.0	14.0
75.48-7	2.6	22.	-0.0	0.00	0.08	3	-0.05	95.	4.1	-0.03	95.	4.1

5.51		1	6					9			9	
75.51-75.53	2.9	17.1	-0.06	0.02	0.08	3	-0.05	94.1	5.9	-0.02	94.1	5.9
76.00-76.03	4.1	17.4	0.06	0.06	0.08	3	0.09	91.9	8.1	0.14	91.9	8.1
76.03-76.08	7.7	18.6	0.06	0.09	0.09	3	0.12	85.5	14.5	0.21	85.5	14.5
76.91-76.96	3.4	21.6	0.04	0.05	0.08	3	0.06	94.6	5.4	0.09	94.6	5.4
76.91-76.96 (dol)	2.8	19.3	0.03	0.09	0.09	3	0.04	94.9	5.1	0.07	94.9	5.1

Note. Average upper crust data is from McLennan (2001).

[a] "dol" = shale material adjacent to dolomite veinlet.

[b] Reported uncertainty for $\delta^{238}U$ is the 2SD of replicate measurements or 0.08‰, whichever is greater.

[c] Authigenic U isotope composition.

[d] Detrital U isotope composition.

[e] Fraction of authigenic U.

[f] Fraction of detrital U.

1198 Table 3. Flux and U isotope fractionation associated with non-anoxic sinks.

Sink	Flux(10^6 mol/yr)	Fractionation	References
Pelagic clay	3	0.04	(1)
Metallic sediments	1	-0.24	(1) to (4)
Carbonates	5.6	0.20	(5) to (7)
Oceanic crustal alteration (High T)	2	0.00	(8) to (10)
Oceanic crustal alteration (Low T)	3.8	0.25	(8) to (10)
Coastal zone retention	7.6	-0.24	(9)
Suboxic (weakly oxygenated seafloor)	15.3	0.10	(2), (11)
Weighted average (oxic)		0.01	
Weighted average (oxic + suboxic)		0.04	

1199 Modified from Wang et al., 2016. The fractionation factor for pelagic clays is poorly

1200 constrained.

1201 References: (1) Wang et al., 2016; (2) Weyer et al., 2008; (3) Brennecka et al., 2011b; (4)

1202 Goto et al., 2014; (5) Romaniello et al., 2013; (6) Stirling et al., 2015; (7) Chen et al., 2016;

1203 (8) Andersen et al., 2015; (9) Tissot and Dauphas, 2015; (10) Noordmann et al., 2016; (11)

1204 Andersen et al., 2016

1205

1206 Table 4. Summary of the parameters used in the U isotope mass-balance model.

Parameter	Description	Values	Unit	References
F_r	Riverine U fluxes to oceans	4.2×10^7	mol/yr	(1) to (4)
F_{ox}	Removal flux to oxic sinks	2.23×10^7	mol/yr	(1) to (4)
$F_{suboxic}$	Removal flux to suboxic sinks	1.53×10^7	mol/yr	(1) to (4)
F_{anoxic}	Removal flux to anoxic sinks	4.45×10^7	mol/yr	(1) to (4)
k_{ox}	Effective burial rate constant for oxic sinks	0.048	1/(dm* yr)	(5)
$k_{suboxic}$	Effective burial rate constant for suboxic sinks	0.469	1/(dm* yr)	(5)
k_{anoxic}	Effective burial rate constant for anoxic sinks	2.534	1/(dm* yr)	(5)
δ_r	$\delta^{238}U$ of river waters	-0.34	‰	(4), (6), (7)
Δ_{ox}	Fractionation factor between seawater and oxic sink	0.01	‰	(5)
$\Delta_{suboxic}$	Fractionation factor between seawater and suboxic sink	0.10	‰	(6), (8)
Δ_{anox}	Fractionation factor between seawater and anoxic sink	0.60-0.85	‰	see text
$[U]_{modern}$	Modern seawater U concentration	1.39×10^{-8}	mol/dm^3	(8), (9)
δ_{modern}	Modern seawater $\delta^{238}U$	-0.4	‰	(4), (8), (10)

V	Seawater volume	1.37×10^{21}	dm^3	(11)
A	Total seafloor area	3.61×10^{16}	dm^3	(1)
	Modern anoxic seafloor area	0.35	%	(12)
	Modern suboxic seafloor area	6	%	(2)
	Modern oxic seafloor area	93.65	%	Balance

Modified from Wang et al., 2016.

References: (1) Barnes and Cochran, 1990; (2) Dunk et al., 2002; (3) Morford and Emerson, 1999; (4) Tissot and Dauphas, 2015; (5) Wang et al., 2016; (6) Andersen et al., 2016; (7) Noordmann et al., 2016; (8) Weyer et al., 2008; (9) Chen et al., 1986; (10) Stirling et al., 2007; (11) Hastings et al., 1996; (12) Veeh, 1967.

Highlights:

- U isotope data from black shales point to increased ocean oxygenation at 1.36 Ga
- A U isotope mass-balance model suggests <25% seafloor anoxia during this event
- Elevated Mo and U enrichments in these shales also support an oxygenation event
- Post-depositional hydrothermal alteration can affect U isotopes in black shales